

AD-A078 439

PRATT AND WHITNEY AIRCRAFT GROUP WEST PALM BEACH FL 6--ETC F/G 21/5
INVESTIGATION OF FAN BLADE SHROUD MECHANICAL DAMPING.(U)

UNCLASSIFIED

JUN 79 D A RIMKUNAS , H M FRYE
PWA-FR-11065

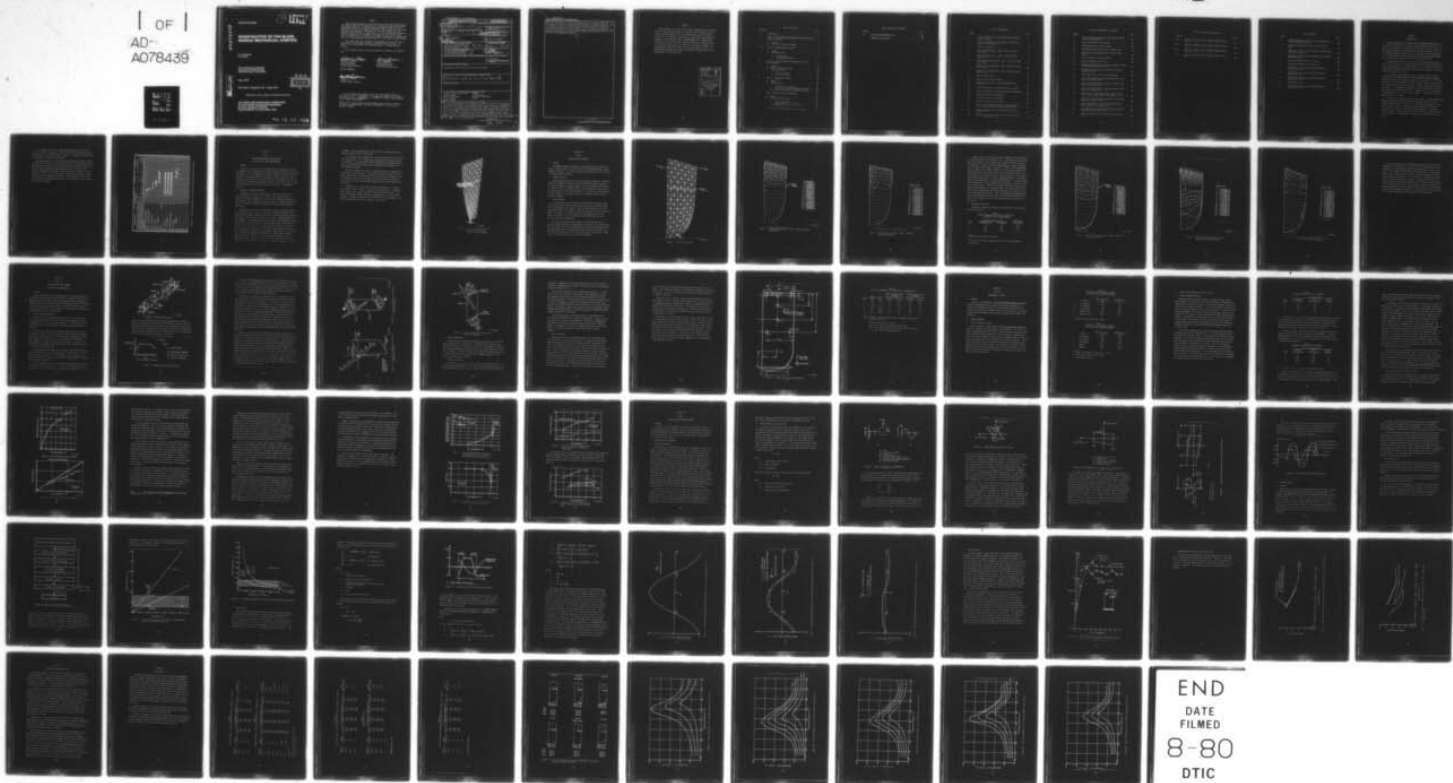
AFAPL-TR-79-2054

F33615-77-C-2086

NL

1 OF 1
AD-
A078439

1



END
DATE
FILMED
8-80
DTIC

AD A 0 7 8 4 3 9

DAC FILE COPY

AFAPL-TR-79-2054

2 LEVEL

INVESTIGATION OF FAN BLADE SHROUD MECHANICAL DAMPING

D. A. Rimkunas
H. M. Frye

Pratt & Whitney Aircraft Group
Government Products Division
West Palm Beach, Florida 33402

June 1979

Final Report 1 September 1977 - 1 March 1979

DDC
RECEIVED
DEC 14 1979
A

APPROVED FOR PUBLIC RELEASE; DISTRIBUTION UNLIMITED

AIR FORCE AERO PROPULSION LABORATORY
Air Force Wright Aeronautical Laboratories
Air Force Systems Command
Wright-Patterson Air Force Base, Ohio


79 12 12 048


NOTICE

When Government drawings, specifications, or other data are used for any purpose other than in connection with a definitely related Government procurement operation, the United States Government thereby incurs no responsibility nor any obligation whatsoever; and the fact that the government may have formulated, furnished, or in any way supplied the said drawings, specifications, or other data, is not to be regarded by implication or otherwise as in any manner licensing the holder or any other person or corporation, or conveying any rights or permission to manufacture, use, or sell any patented invention that may in any way be related thereto.

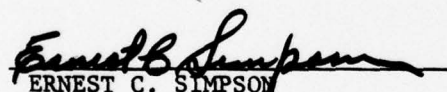
This report has been reviewed by the Information Office (OI) and is releasable to the National Technical Information Service (NTIS). At NTIS, it will be available to the general public, including foreign nations.

This technical report has been reviewed and is approved for publication.


WILLIAM A. STANGE
Project Engineer
Propulsion Branch
Turbine Engine Division


ISAK J. GERSHON
Acting Branch Chief
Propulsion Branch
Turbine Engine Division

FOR THE COMMANDER


ERNEST C. SIMPSON
Director
Turbine Engine Division

If your address has changed, if you wish to be removed from our mailing list, or if the addressee is no longer employed by your organization please notify AFAPL/TBP, W-PAFB, OH 45433 to help us maintain a current mailing list.

Copies of this report should not be returned unless return is required by security considerations, contractual obligations, or notice on a specific document.

UNCLASSIFIED

SECURITY CLASSIFICATION OF THIS PAGE (When Data Entered)

| (19) REPORT DOCUMENTATION PAGE | | READ INSTRUCTIONS BEFORE COMPLETING FORM | |
|--|-----------------------|--|--|
| 1. REPORT NUMBER (18) AFAPL-TR-79-2054 | 2. GOVT ACCESSION NO. | 3. RECIPIENT'S CATALOG NUMBER | |
| 4. TITLE (and Subtitle) (6) INVESTIGATION OF FAN BLADE SHROUD MECHANICAL DAMPING | | 5. TYPE OF REPORT & PERIOD COVERED Technical Final 9-1-77 through 3-1-79 | |
| 6. AUTHOR(s) (10) Donald A. Rinkunas H. Frye (MURPHY) | | 7. PERFORMING ORG. REPORT NUMBER (14) PWA-FR-11065 | |
| 8. PERFORMING ORGANIZATION NAME AND ADDRESS Pratt & Whitney Aircraft Group Government Products Division West Palm Beach, FL 33402 | | 9. CONTRACT OR GRANT NUMBER(s) (15) F33615-77-C-2086 | |
| 10. CONTROLLING OFFICE NAME AND ADDRESS AF Aero Propulsion Laboratory (TBP) Air Force Systems Command Wright-Patterson AFB, Ohio 45433 | | 11. PROGRAM ELEMENT, PROJECT, TASK AREA & WORK UNIT NUMBERS (12) 79 (16) 2307-S2-03 (17) S2 | |
| 12. MONITORING AGENCY NAME & ADDRESS (if different from Controlling Office) 15611025 | | 13. REPORT DATE (11) Jun 79 | |
| | | 14. SECURITY CLASS. (of this report) UNCLASSIFIED | |
| | | 15a. DECLASSIFICATION/DOWNGRADING SCHEDULE | |
| 16. DISTRIBUTION STATEMENT (of this Report) Approved for Public Release; Distribution Unlimited 392 887 | | | |
| 17. DISTRIBUTION STATEMENT (of the abstract entered in Block 20, if different from Report) (9) Final Rept. 1 Sep 77-1 Mar 79 | | | |
| 18. SUPPLEMENTARY NOTES | | | |
| 19. KEY WORDS (Continue on reverse side if necessary and identify by block number) YF100(I) Trailing Edge Shroud NASTRAN Shroud Loading Vibration Mode Fully-locked Shroud Analytical Predictions Gross Slipping Airfoil Micro-slipping | | | |
| 20. ABSTRACT (Continue on reverse side if necessary and identify by block number) This program was conducted to investigate the effect of dry friction damping at the shroud interfaces on the structural dynamic characteristics of shrouded fan blades typical of current high performance jet engines. An analytical definition of the loads generated at the shroud faces for a general stick-slip condition was developed. The analytical load description includes the elastic case of a stuck or locked shroud as well as the case of a slipping shroud. These loads were used in a non-linear steady-state vibration analysis of the shrouded blade. Controlled vibration testing of the first-stage fan blade with a | | | |

DD FORM 1 JAN 73 1473 EDITION OF 1 NOV 65 IS OBSOLETE

UNCLASSIFIED

SECURITY CLASSIFICATION OF THIS PAGE (When Data Entered)

392 887

over
slk

UNCLASSIFIED

SECURITY CLASSIFICATION OF THIS PAGE(When Data Entered)

trailing edge shroud of a YF100 (prototype) turbofan engine was conducted. The blade was tested with variable shroud restraints to simulate the full range of boundary conditions from freely slipping to fully locked, including the intermediate condition of micro-slipping. The testing of the blade with a freely slipping shroud was inconclusive because of repeatability problems. Good agreement was found between the nonlinear analysis and test data for the stuck and micro-slip boundary conditions.

UNCLASSIFIED

SECURITY CLASSIFICATION OF THIS PAGE(When Data Entered)

PREFACE

The following is a final technical report documenting work performed under Air Force Contract F33615-77-C-2086 by Pratt & Whitney Aircraft Group Government Products Division (P&WA/Florida), United Technologies Corporation. The program, "Investigation of Fan Blade Shroud Mechanical Damping," was an 18-month effort (from September 1977 to March 1979) sponsored by the Air Force Aero Propulsion Laboratory, Wright-Patterson Air Force Base, Ohio, under the cognizance of William A. Stange, Project Engineer, Propulsion Branch of the Turbine Engine Division. The P&WA/Florida Principal Investigator was Donald A. Rimkunas and the Program Manager was H. Murray Frye.

| | |
|--------------------|-------------------------------------|
| Accession For | |
| NTIS GMA&I | <input checked="" type="checkbox"/> |
| DDC TAB | <input type="checkbox"/> |
| Unannounced | <input type="checkbox"/> |
| Justification | |
| By _____ | |
| Distribution/ | |
| Availability Codes | |
| Dist | Avail and/or special |
| A | |

TABLE OF CONTENTS

| SECTION | | PAGE |
|---------|---|------|
| I | INTRODUCTION | 1 |
| II | TASK I FINITE ELEMENT MODEL MODIFICATION AND ANALYTICAL SYSTEM DEVELOPMENT | 4 |
| | A. General | 4 |
| | B. Analytical System Development | 4 |
| III | TASK II, COMPUTER MODEL ANALYSIS | 7 |
| | A. General | 7 |
| | B. NASTRAN Analysis | 7 |
| | 1. Vibration Modes | 7 |
| | 2. Frequencies Predicted | 11 |
| IV | TASK III, TEST PROCEDURES AND HARDWARE DEFINITION AND PROCUREMENT | 16 |
| | A. General | 16 |
| | B. Shroud Load Distributions | 16 |
| | C. Testing Procedures | 20 |
| | 1. Initial Test Phase | 20 |
| | 2. Final Test Phase | 21 |
| V | TASK IV, EXPERIMENTAL TESTING | 25 |
| | A. General | 25 |
| | B. Testing Process | 25 |
| | 1. Initial Fan Blade Testing | 25 |
| | 2. Initial Testing Phase of Single Fan Blade | 27 |
| | 3. Final Testing Phase of Single Fan Blade | 29 |
| VI | TASK V, DATA ANALYSIS AND CORRELATION | 36 |
| | A. General | 36 |
| | B. Analytical Model Analysis | 36 |
| | 1. General Background | 36 |
| | 2. Blade Shroud Stick Slip Analysis | 37 |
| | 3. NASTRAN Analysis | 42 |
| | C. Comparison of Analytical Data to Test Data | 55 |

TABLE OF CONTENTS (CONTINUED)

| SECTION | | PAGE |
|---------|---------------------------------------|------|
| VII | CONCLUSIONS/RECOMMENDATIONS | 58 |
| | APPENDIX, TEST RESULTS. | 59 |

LIST OF ILLUSTRATIONS

| Figure | | Page |
|--------|---|------|
| 1 | Program Schedule for the Fan Blade Shroud Damping Analysis Program | 3 |
| 2 | Finite Element Model of the YF100(I) Trailing-Edge-Shroud First-Stage Blade | 6 |
| 3 | Airfoil Idealization | 8 |
| 4 | Blade With Ring Shroud - Mode 1 Analytical Modal Displacement | 9 |
| 5 | Blade With Ring Shroud - Mode 2 Analytical Modal Displacement | 10 |
| 6 | Blade With Slipping Shroud - Mode 1 Analytical Modal Displacement | 12 |
| 7 | Blade With Slipping Shroud - Mode 2 Analytical Modal Displacement | 13 |
| 8 | Blade With Slipping Shroud - Mode 3 Analytical Modal Displacement | 14 |
| 9 | Shroud Loading Device | 17 |
| 10 | Normal Shroud Load Distribution | 17 |
| 11 | Restrained Grid Points at Airfoil/Shroud Inter-section | 19 |
| 12 | Load Distribution for Shroud Restrained at Airfoil . . | 19 |
| 13 | Load Distribution for Shroud and Airfoil Interaction . | 20 |
| 14 | Location of Blade Instrumentation | 23 |
| 15 | Stress/Excitation in First Mode | 30 |
| 16 | Stress/Excitation in Torsion Mode | 30 |
| 17 | Phase Relation Between Tip to Root Accelerometers in First Bending Mode versus Input Excitation Level . . . | 34 |
| 18 | Frequency versus Input Excitation Level for First Bending Mode | 34 |
| 19 | Percent of Critical Damping versus Input Excitation for a Constant Shroud Load | 35 |

LIST OF ILLUSTRATIONS (Continued)

| Figure | | Page |
|--------|--|------|
| 20 | Percent of Critical Damping versus Input Excitation for First Bending Mode | 35 |
| 21 | Simple One-Degree-of-Freedom Model | 38 |
| 22 | Blade Motion Versus Slip at Shroud | 39 |
| 23 | Blade Motion Versus Shear Force at Shroud Face | 40 |
| 24 | Transition From Slipping Shroud to Fully Locked Shroud | 41 |
| 25 | Force Variation at Shroud Interface | 42 |
| 26 | Analysis Procedure Flow Chart | 44 |
| 27 | Analytical Prediction of the Effect of Normal Shroud Load on Shroud Interface Motion | 45 |
| 28 | The Effect of Coefficient of Friction on Shroud Interface Motion | 46 |
| 29 | Local Shroud Force for Stick-Slip Condition | 48 |
| 30 | Analytical Representation of Shroud Interface Load Over a Cycle Where $\mu N/KU = 1$ | 50 |
| 31 | Analytical Representation of Shroud Interface Load Over a Cycle Where $\mu N/KU = 0.5$ | 51 |
| 32 | Analytical Representation of Shroud Interface Load Over a Cycle Where $\mu N/KU = 0.1$ | 52 |
| 33 | Analytical Predicted Normal Displacement at Blade Tip $\omega = 345$ Hz, Normal Shroud Load: $N=234$ lb | 54 |
| 34 | Analytical and Test Results Comparison of Blade Tip Response vs Input Excitation | 56 |
| 35 | Blade Tip Response vs Input Excitation For Given Shroud Normal Loads During Testing | 57 |
| 36 | Blade Mode Shapes and Frequency from Bench Testing With Shrouds Restrained at 234 lb | 63 |
| 37 | Blade Tip Response versus Frequency Shroud Load at 200 lb | 64 |

LIST OF ILLUSTRATIONS (Continued)

| Figure | | Page |
|--------|--|-------|
| 38 | Blade Tip Response versus Frequency Shroud Load at 234 lb | 65 71 |
| 39 | Blade Tip Response versus Frequency Shroud Load at 280 lb | 66 72 |
| 40 | Blade Tip Response versus Frequency Shroud Load at 330 lb | 67 73 |
| 41 | Blade Tip Response versus Frequency Shroud Load at 400 lb | 68 74 |

LIST OF TABLES

| Table | | Page |
|-------|---|-------|
| 1 | Natural Frequencies of YF100(I) First-Stage Blade With Trailing Edge Shroud | 11 |
| 2 | Analytical Prediction of Stress Level at Shroud Slip | 24 |
| 3 | Analytical vs Test Natural Frequency for Blade With Unrestrained Shroud | 26 |
| 4 | Analytical vs Test Natural Frequency for Balde With Restrained Shroud | 26 |
| 5 | Unrestrained Shroud Blade Test Results | 28 |
| 6 | Restrained Shroud Blade Test Results | 28 |
| 7 | Fan Blade Testing in First Bending Mode With a Shroud Load = 200 lb | 60 66 |
| 8 | Fan Blade Testing in First Bending Mode With a Shroud Load = 234 lb | 60 66 |
| 9 | Fan Blade Testing in First Bending Mode With a Shroud Load = 280 lb | 61 67 |
| 10 | Shroud Load 330 lb | 61 67 |
| 11 | Fan Blade Testing in First Bending Mode With a Shroud Load = 400 lb | 62 68 |

SECTION I

INTRODUCTION

The proper design of rotor blades used in high performance gas turbine engines is dependent on high cycle fatigue failure avoidance. This in turn, is contingent on the accurate prediction of flutter instability and resonant response to distorted inlet flow and vane wakes. Analytical techniques used to predict flutter and resonant stress designs rely on accurately defined structural dynamic characteristics of the bladed disk as related to the contact surfaces at part span shrouds.

During engine operation, the shrouds of adjacent fan blades may remain in contact and act as a continuous ring, or the shrouds may experience relative motion at the contact surfaces. In the latter, the resultant slipping and Coulomb friction forces may dissipate significant vibratory energy which damps the motion.

The Fan Blade Shroud Damping Analysis program, Contract F33615-77-C-2086, was an 18-month effort as discussed in the following document. The purpose was to investigate the effect of dry friction (i.e., Coulomb) damping at the shroud interfaces on the structural dynamic characteristics of shrouded fan blades typical of those currently used in high performance jet engines. The program was conducted by the Pratt & Whitney Aircraft Group of United Technologies with D. A. Rimkunas acting as the Principal Investigator and H. M. Frye as Program Manager. The Air Force Project Engineer was W. A. Stange.

The program was divided into five tasks: Task I - Finite Element Model Modification and Analytical Prediction System Development; Task II - Computer Model Analysis; Task III - Test Procedure and Hardware Definition and Procurement; Task IV - Rig Testing (under experimental laboratory conditions); and Task V - Data Analysis and Correlation. Additional efforts involved the publishing of monthly activity reports and the final technical report. This document is organized to reflect specific task efforts.

This document reflects the effort conducted under the referenced contract to address the problem of properly modeling the dynamic mechanical behavior of a fan blade shroud. Figure 1 illustrates the task breakdown and their sequential accomplishment.

The program objectives were accomplished through controlled vibration testing of the YF100(I) first-stage fan blade with a trailing edge shroud. The blade was tested with variable shroud interface restraints to simulate the full range of boundary conditions from freely slipping to fully locked, including the intermediate condition of micro-slipping. Using a numerical analysis, the test cases were correlated to develop an analytical model of shroud mechanical behavior. This model can be used to improve accuracy in determining fan blade natural frequencies, mode shapes, and mechanical damping.

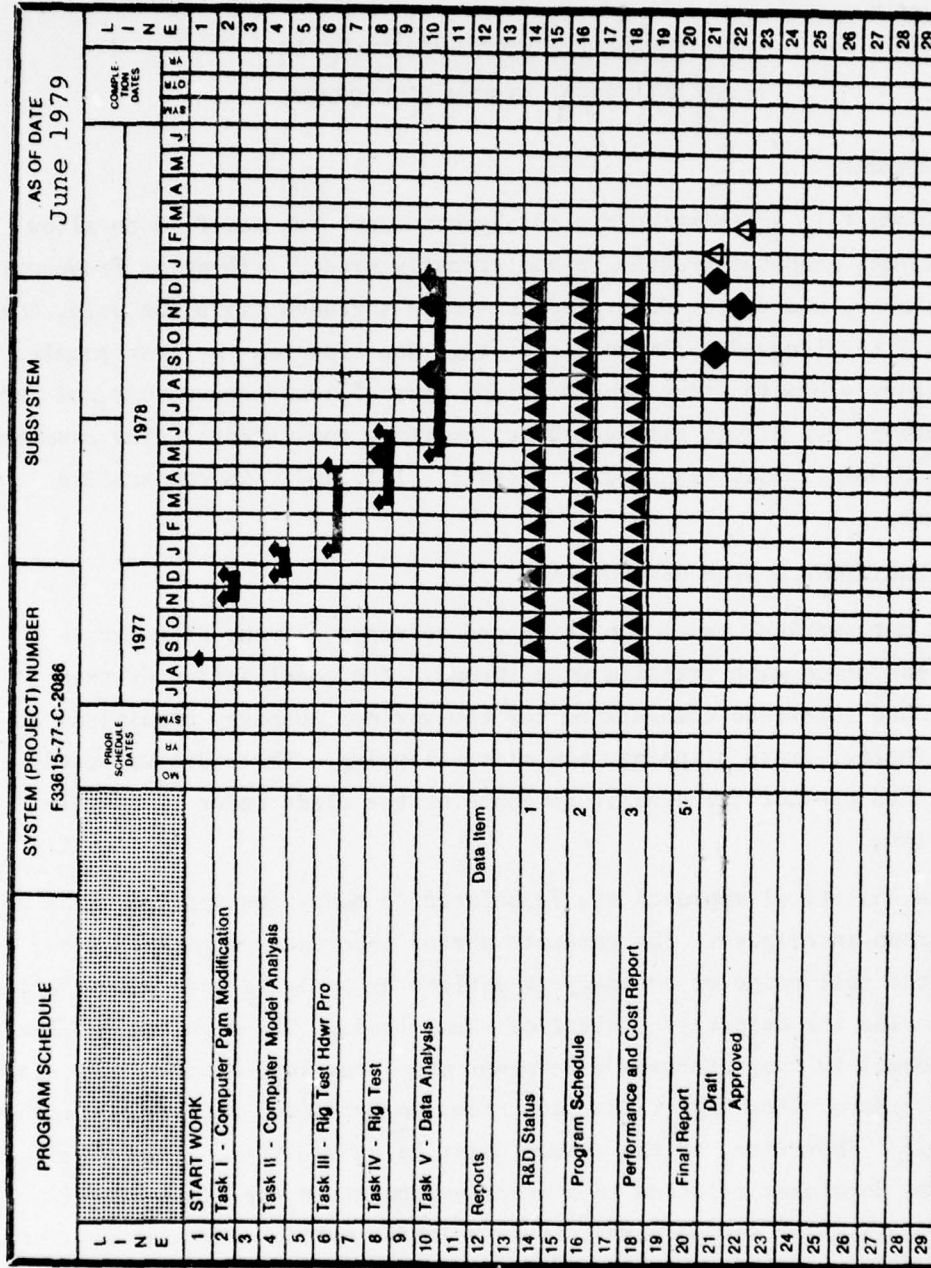


Figure 1. Program Schedule for the Fan Blade Shroud Damping Analysis Program

SECTION II

TASK I

FINITE ELEMENT MODEL MODIFICATION AND ANALYTICAL SYSTEM DEVELOPMENT

A. GENERAL

In Task I, an existing finite element model was modified to allow the NASTRAN computer program to analytically predict vibration frequencies, mode shapes, and system damping of a single shrouded fan blade using the YF100(I) trailing-edge-shroud first-stage fan blade as the test sample. Laboratory vibration testing conditions were at room temperature and zero revolutions per minute with variable interface constraints. The resultant finite element model was used in Tasks II, III, and V in comparative analyses.

B. ANALYTICAL SYSTEM DEVELOPMENT

A mathematical model was developed to represent the F100 first-stage fan blade with trailing edge shroud. The idealization of the shroud and interface compensated for the various boundary conditions of non-slipping, gross slipping, and micro-slipping. The model was used in Task II to predict the dynamic response of the blade under laboratory conditions.

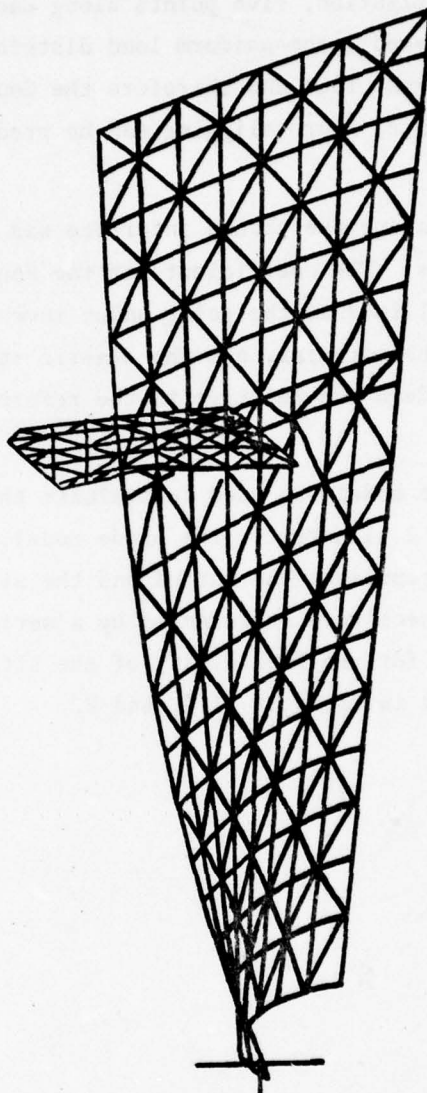
An analytical approach was formulated to model the applied loads at the shroud interfaces. The variable shroud interface restraints simulated the full range of boundary conditions by applying load distributions to describe the respective interface shear loads. The magnitude of the load normal to the interface determines the shear load distribution along the interface. For high values of shroud normal load, the shroud does not slip. Therefore, at the shroud point being analyzed, a linear elastic load was developed relative to a reference point on the blade airfoil. For low values of shroud normal load, relative motion occurs at the interface. Under this condition, the magnitude of shear load is limited to the friction load. Between the freely-slipping and fully-restrained shroud conditions, the normal interface load increases elastically until this elastic load equals the magnitude of the friction load at the shroud

interface. The limiting shroud interface load at a given point on the shroud interface is the friction load.

In the analytical investigation, five points along each of the interfaces were chosen. This allowed a non-uniform load distribution along the interface. Since the normal load and therefore the Coulomb friction forces vary along the interface, micro-slipping can be predicted with this mathematical model.

The load at each point along the shroud interface was mathematically described by a Fourier series. The coefficients of the Fourier series were a function of the normal load at the point under investigation, the coefficient of friction of the material, and the elastic stiffness of the shroud point under consideration relative to the referenced point on the airfoil.

A NASTRAN finite element model was used to evaluate the stiffness of the blade shroud. Figure 2 illustrates the blade model. Triangular plate elements were used to represent the shroud and the airfoil. The blade platform and extended neck were represented by a series of beam elements. Springs accounted for the flexibility of the attachment. This finite element model was used in Tasks II, III, and V.



FD 148417

Figure 2. Finite Element Model of the
YF100(I) Trailing-Edge-
Shroud First-Stage Blade

SECTION III

TASK II

COMPUTER MODEL ANALYSIS

A. GENERAL

The NASTRAN computer program was used to analytically predict the normal vibratory modes of the blade for the following degenerate shroud boundary conditions: (1) freely slipping shroud interface, and (2) fully restrained shroud interfaces.

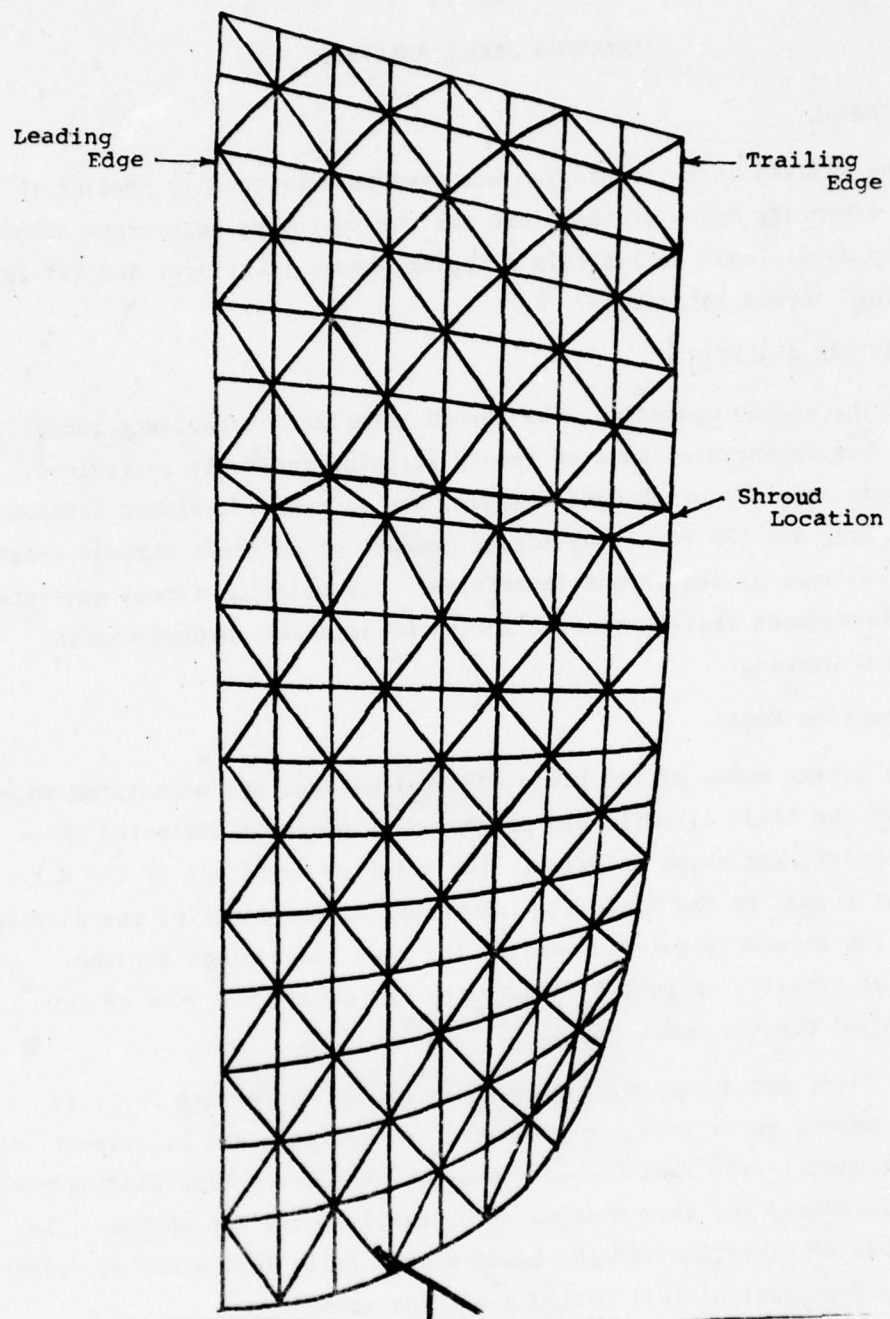
B. NASTRAN ANALYSIS

During engine operation, the shroud interfaces experience conditions between the degenerate cases of freely slipping and fully restrained. Each blade untwists or changes stagger, due to centrifugal and aerodynamic loading, and the resulting forced contact of adjacent shrouds create an applied load at the shroud interfaces. The friction forces generated at the interfaces resist relative motion of adjacent shrouds causing mechanical damping.

1. Vibration Modes

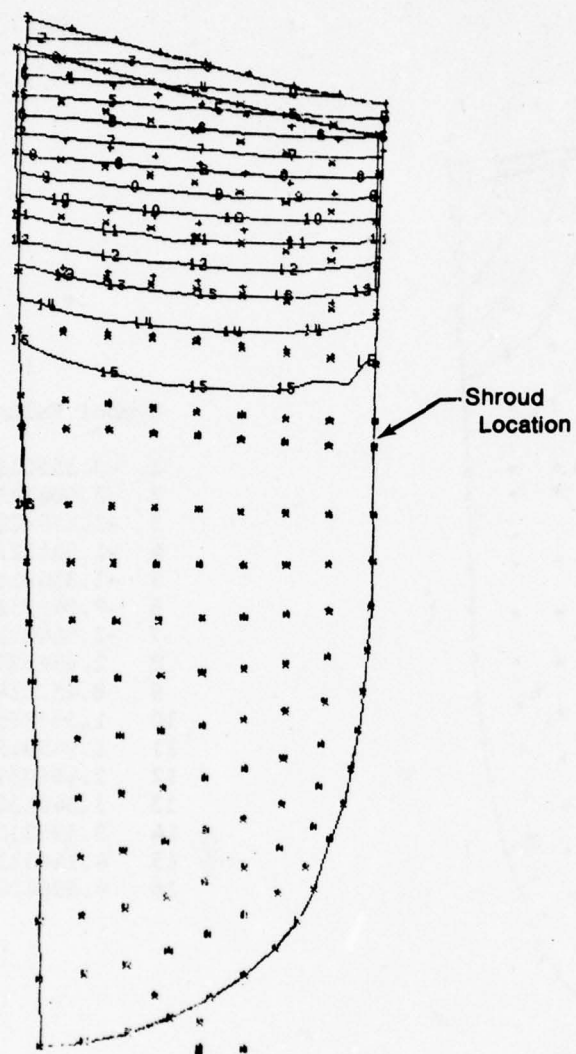
The normal modes of the blade were calculated, and normalized mode shapes of the blade airfoil were presented as plots of deflected shape with a nondeformed shape underlay. The relative magnitude of the displacement normal to the airfoil is shown by contour lines of the displacements. The shroud is not included on the mode shape plots for the purpose of clarity. Figure 3 illustrates the undeformed view of the airfoil used for the modal plots.

The first and second vibration modes of the blade with fully restrained shroud interfaces are presented in Figures 4 and 5, respectively. The first mode is the first bending mode or cantilever beam-bending mode. The displacements for this mode occur primarily above the shroud. The second mode of vibration for the blade with a fully restrained or "ring" shroud is torsional airfoil motion above the shroud.



FD 148418

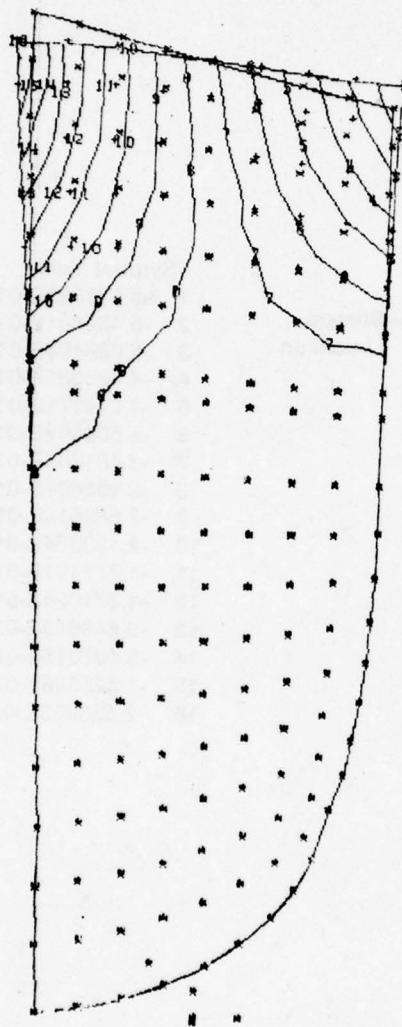
Figure 3. Airfoil Idealization



| Symbol Value | |
|--------------|---------------|
| 1 | -5.838825E-01 |
| 2 | -5.432661E-01 |
| 3 | -5.026498E-01 |
| 4 | -4.620335E-01 |
| 5 | -4.214171E-01 |
| 6 | -3.808008E-01 |
| 7 | -3.401845E-01 |
| 8 | -2.995681E-01 |
| 9 | -2.589518E-01 |
| 10 | -2.183354E-01 |
| 11 | -1.777191E-01 |
| 12 | -1.371028E-01 |
| 13 | -9.648645E-02 |
| 14 | -5.587015E-02 |
| 15 | -1.525386E-02 |
| 16 | 2.536203E-02 |

FD 143542

Figure 4. Blade With Ring Shroud - Mode 1 Analytical Modal Displacement



Symbol Value

| | |
|----|---------------|
| 1 | -3.555015E-01 |
| 2 | -3.004919E-01 |
| 3 | -2.454823E-01 |
| 4 | -1.904727E-01 |
| 5 | -1.354631E-01 |
| 6 | -8.045352E-02 |
| 7 | -2.544392E-02 |
| 8 | 2.956587E-02 |
| 9 | 8.457524E-02 |
| 10 | 1.395848E-01 |
| 11 | 1.945943E-01 |
| 12 | 2.496039E-01 |
| 13 | 3.046134E-01 |
| 14 | 3.596230E-01 |
| 15 | 4.146325E-01 |
| 16 | 4.696424E-01 |

FD 148419

Figure 5. Blade With Ring Shroud - Mode 2 Analytical
Modal Displacement

Figures 6 and 7 illustrate the first two modes of the blade when the shroud interfaces are allowed to slip. The shrouds are restrained from motion normal to the interface but allowed to deflect parallel to the interface. For the slipping shroud conditions, Figure 6 presents the first mode of the blade. This mode is a basic first beam-bending vibration mode. The slipping shrouds allow the blade to deform from approximately 50% of the span to the tip; the ring shroud limits the displacement of the airfoil primarily above the shroud. The second vibratory mode of the blade with freely slipping shrouds is a cantilever beam second bending mode, as illustrated in Figure 7. Further analysis of the blade with a freely-slipping shroud showed the third mode to be above shroud torsion. Figure 8 illustrates the third analytical mode shape for the blade with a slipping shroud. The above-shroud torsion mode was the second mode analytically predicted for a blade with the ring shroud boundary condition. Thus, increasing the shroud restraint causes the above-shroud-torsion mode to move from the third mode of a blade with a slipping shroud to the second mode of the blade with a ring shroud.

2. Frequencies Predicted

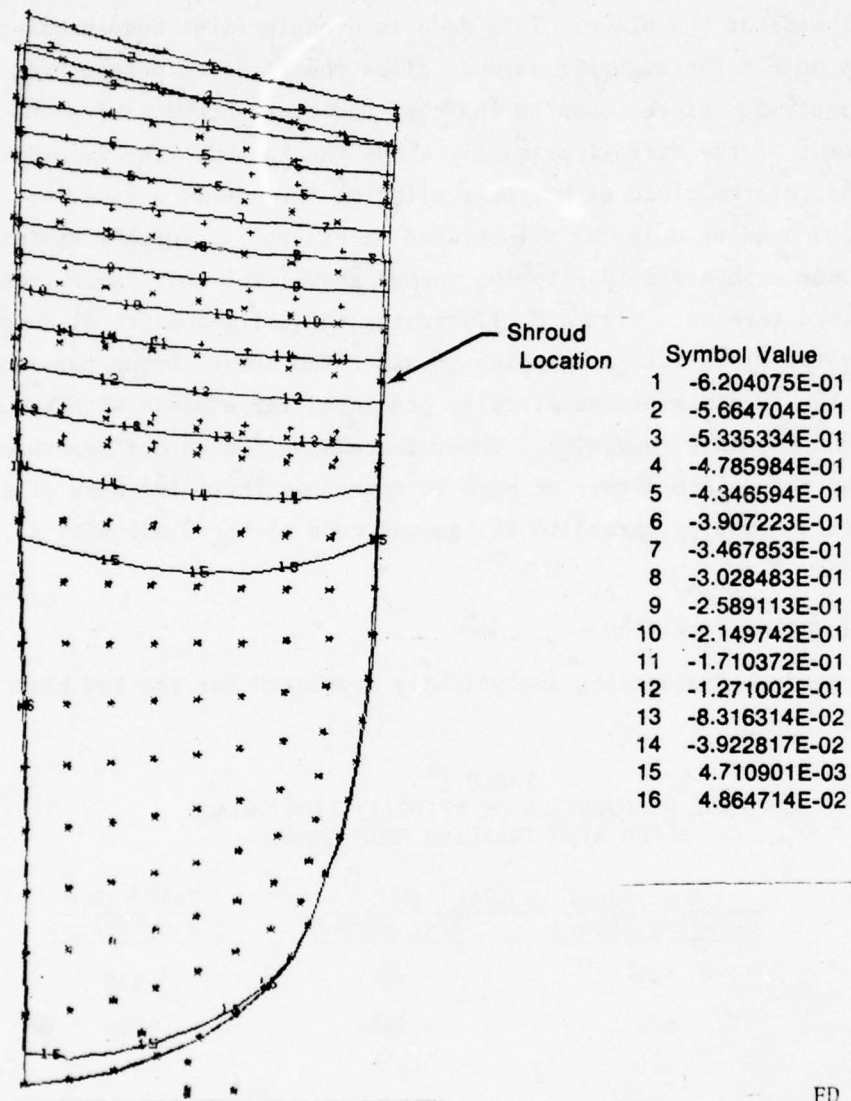
The natural frequencies analytically predicted for the fan blade are shown in Table 1.

TABLE 1.
NATURAL FREQUENCIES OF YF100(I) FIRST-STAGE
BLADE WITH TRAILING EDGE SHROUD

| Mode | Analytical Results ¹ (Hz) | | Test ² (Hz) |
|------|--------------------------------------|-------------|------------------------|
| | Slipping Shroud | Ring Shroud | Ring Shroud |
| 1 | 183 | 351 | 370 |
| 2 | 622 | 993 | 1005 |
| 3 | 980 | 1378 | — |

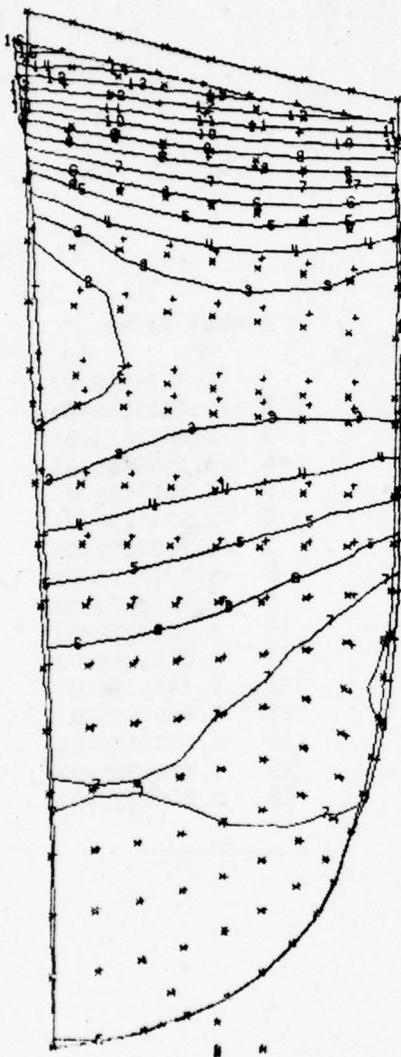
¹NASTRAN finite element predictions.

²Blade alone test data, shroud load at 450 in.-lb (ring shroud simulation).



FD 143541

Figure 6. Blade With Slipping Shroud - Mode 1 Analytical Modal Displacement

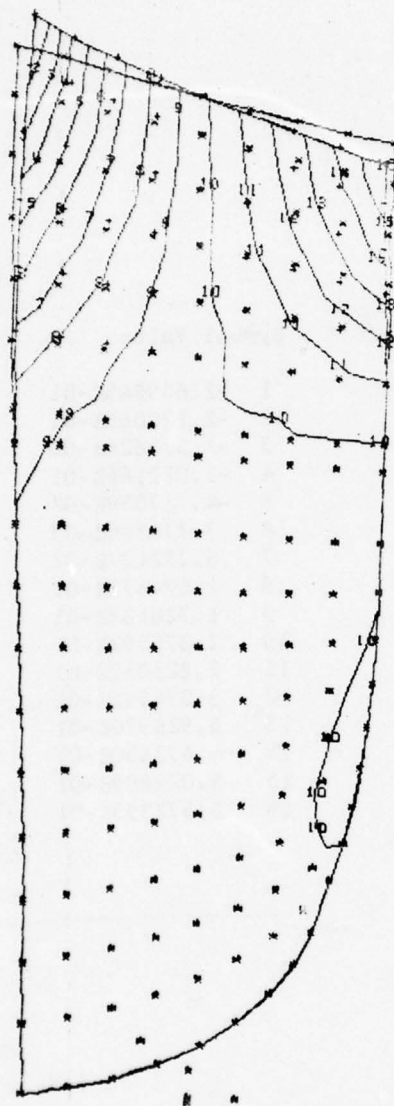


Symbol Value

| | |
|----|---------------|
| 1 | -2.669546E-01 |
| 2 | -2.120086E-01 |
| 3 | -1.570626E-01 |
| 4 | -1.021166E-01 |
| 5 | -4.717059E-02 |
| 6 | 7.775396E-03 |
| 7 | 6.272137E-02 |
| 8 | 1.176673E-01 |
| 9 | 1.726133E-01 |
| 10 | 2.275592E-01 |
| 11 | 2.825052E-01 |
| 12 | 3.374511E-01 |
| 13 | 3.923970E-01 |
| 14 | 4.473430E-01 |
| 15 | 5.022889E-01 |
| 16 | 5.572353E-01 |

FD 148420

Figure 7. Blade With Slipping Shroud - Mode 2
Analytical Modal Displacement



Symbol Value

| | |
|----|---------------|
| 1 | -4.707487E-01 |
| 2 | -4.176314E-01 |
| 3 | -1.645141E-01 |
| 4 | -3.113968E-01 |
| 5 | -2.582798E-01 |
| 6 | -2.051623E-01 |
| 7 | -1.520459E-01 |
| 8 | -9.892774E-02 |
| 9 | -4.581047E-02 |
| 10 | 7.308792E-03 |
| 11 | 6.042406E-02 |
| 12 | 1.135413E-01 |
| 13 | 1.666585E-01 |
| 14 | 2.197757E-01 |
| 15 | 2.728930E-01 |
| 16 | 3.260103E-01 |

FD 148421

Figure 8. Blade With Slipping Shroud - Mode 3
Analytical Modal Displacement

Table 1 shows the first three modes of vibration calculated by the NASTRAN finite element model. Both the freely-slipping and the fully restrained, or ring shroud, boundary condition analytical results are given. Also shown are existing test data which reflect a blade with a normal shroud load that causes a 450 in.-lb untwist moment to simulate engine operating conditions. The second mode of vibration during the test was the above-shroud-torsion mode. This indicated that at this shroud load during previous testing, the blade acted in a manner similar to the analytical blade with a ring shroud. A comparison between the natural frequencies of the existing test data and the analytical prediction showed the frequencies agreed. This indicated that the analytical finite element model adequately represented the actual blade.

SECTION IV

TASK III

TEST PROCEDURES AND HARDWARE

DEFINITION AND PROCUREMENT

A. GENERAL

Task III provided for the establishment of testing procedures and testing hardware definition and procurement. Using three YF100(I) fan blades with trailing edge shrouds, test parameters such as frequency, amplitude, and level of shroud constraint loads were defined. The application of sensors were defined, methods of applying shroud load constraints were determined, and procedures for calibrating instrumentation and conducting tests were established.

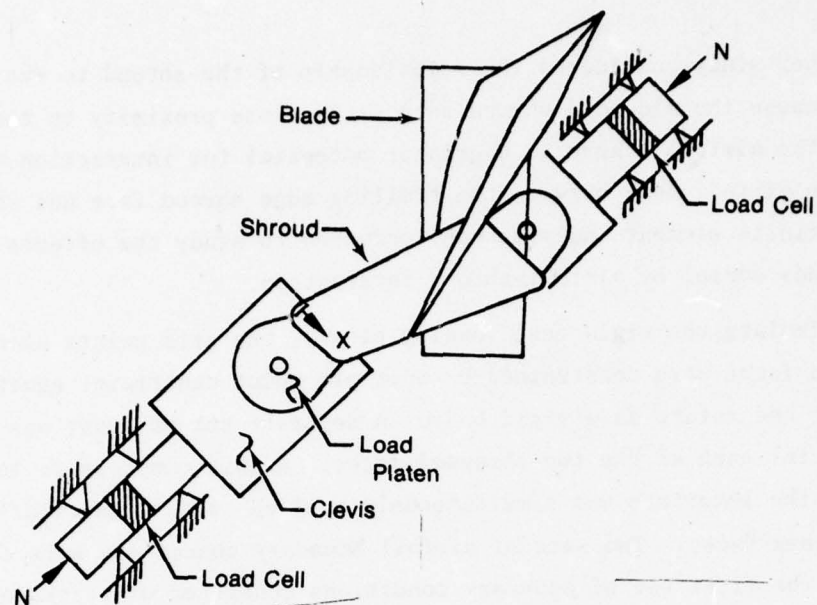
B. SHROUD LOAD DISTRIBUTIONS

The elastic shear load distribution relative to the frictional shear loads generated at the shroud interface determines the amount of slippage which occurs at the shroud interface. To determine the frictional shear loads along the shroud, the normal load distribution is required.

Figure 9 is a diagram of the shroud loading device used in the laboratory testing. The fixture consists of two clevises constrained to move in a straight line. Each clevis supports a load platen which bears against the shroud face. As the clevises are moved forward, the load platens are allowed to rotate as they translate. Thus, as the blade rotates and deflects under shroud loads, the load platen is held in contact with the shroud face.

The load distribution under test conditions was analytically determined by performing a static NASTRAN analysis of the blade. The blade was restrained from motion at the attachment. The grid points along each of the shroud faces were connected with a rigid element (a multiple-point constraint equation).

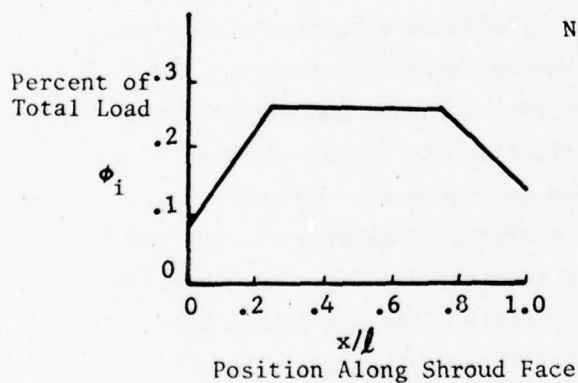
A unit deflection normal to the shroud face was applied at the center of each shroud and the reaction required to cause the displacement calculated. This reaction was used to normalize the load at each grid



FD 143547

Figure 9. Shroud Loading Device

point on the blade shroud face yielding the normal load distribution. Figure 10 illustrates the normal load distribution along the trailing edge shroud interface for the laboratory test conditions. Because the friction force is proportional to the normal load, the load distribution shown in Figure 10 indicates that the friction force will be maximum at the center and minimum at the edges of the shroud.



$$N_i = \phi_i N$$

Where:

N_i = Load at Grid

N = Total Load at Shroud

l = Length of Shroud Face

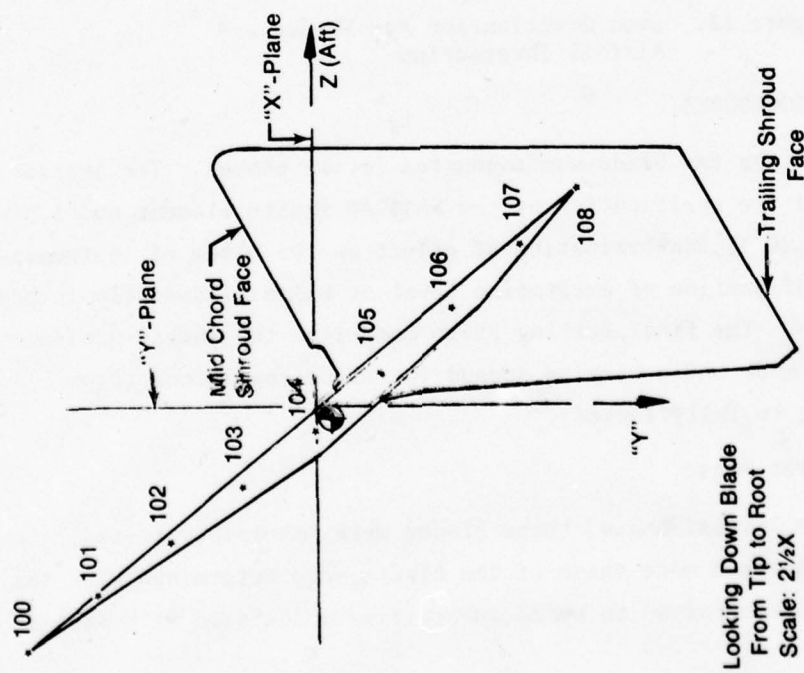
x = Position on Shroud

Figure 10. Normal Shroud Load Distribution

Further study considered the relationship of the shroud to the airfoil. Because the midchord shroud face is in close proximity to the midchord of the airfoil, there is a greater potential for interaction between it and the airfoil than between the trailing edge shroud face and the airfoil. A finite element analysis was conducted to study the effects on shroud loads caused by airfoil-shroud interaction.

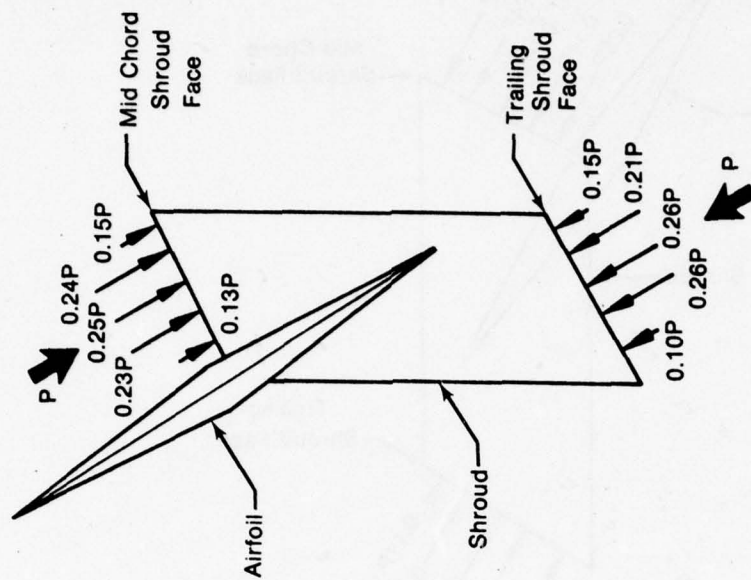
To simulate the rigid test loading blocks, the grid points along the shroud faces were constrained by multiple point constraint equations to deflect and rotate as a rigid body. A separate set of equations was developed for each of the two shrouded faces. A unit compressive load normal to the interface was simultaneously applied to the center of each of the shroud faces. Two sets of airfoil boundary conditions were considered. The first set of boundary conditions consisted of restraining the airfoil at the intersection with the shroud. These restrained airfoil grid points are indicated by points 104 through 108 in Figure 11. The second set consisted of restraining the airfoil at its root from all motion, allowing the entire blade to deform. The analysis yielded the resultant grid point forces along each of the shroud faces, thus giving the load distribution across each of the shroud faces for the two boundary conditions.

Figure 12 illustrates the distribution of the total applied unit load to the shroud faces with the airfoil restrained at the shroud-airfoil junction. This pattern of grid point loads yields an essentially uniform compressive stress field adjacent to the shroud faces. Restraining the airfoil at the blade root and allowing the entire shroud and airfoil to deform had little effect on the load distribution of the shroud face nearest the airfoil trailing edge, as shown in Figure 13. However, the midchord shroud face, being closer to the airfoil, is materially affected by the interaction between the airfoil and the shroud. Thus, the location of the shroud relative to the airfoil can greatly alter the shroud load distribution and the resultant potential for shroud slippage. The normal load distribution illustrated in Figure 13 was used for the analytical determination of shroud shear loads.



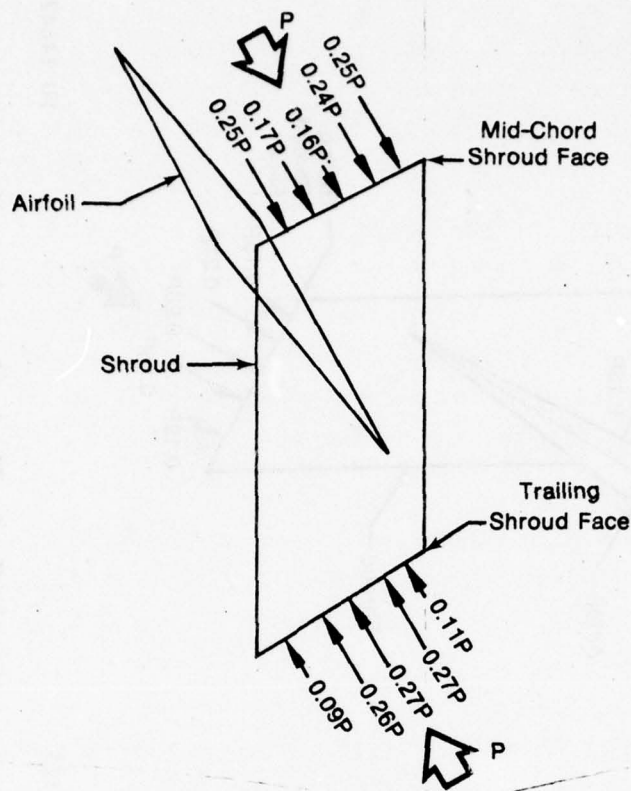
FD 148423

Figure 11. Restrained Grid Points at Airfoil/
Shroud Intersection



FD 148424

Figure 12. Load Distribution for Shroud Re-
strained at Airfoil



FD 148425

Figure 13. Load Distribution for Shroud and Airfoil Interaction

C. TESTING PROCEDURES

Testing of the fan blade was conducted in two phases. The initial phase comprised the verification of the NASTRAN finite element model generated in Task II, determination of effect on the blade of instrumentation, and confirmation of excitation level at which blades slip in the first two modes. The final testing phase comprised the investigation of a single blade mode while varying shroud interface conditions (from freely slipping to fully locked).

1. Initial Test Phase

During the initial phase, three blades were laboratory tested. The natural frequency and mode shape of the blades were determined with the blade shrouds unrestrained to avoid ambiguities associated with shroud

modeling. A comparison of the analytical results to the test results was made to demonstrate the validity of the basic airfoil finite element mathematical model (Task I).

The test was repeated with the shroud fully restrained. A normal load of 234 lb was applied to each shroud. This amplitude of normal load develops during typical engine operation and represents a fully restrained condition. Following these tests, the fully restrained shroud test data were compared to the natural frequency and mode shape predicted by the NASTRAN mathematical model (Task II) for a fully restrained shroud. Correlation of these data was made to show the adequacy of the NASTRAN finite element model to accurately depict the shroud and shroud boundary conditions of the blade.

A quantitative measure of the mode shape was determined using seven micro-accelerometers and vibratory strain gages. Figure 14 shows the location of the blade instrumentation. After the instrumentation was added to the blade, the frequency and mode shape were rechecked. Changes in frequency of less than 1½% demonstrated that the small mass added to the blade did not have a significant affect on blade response.

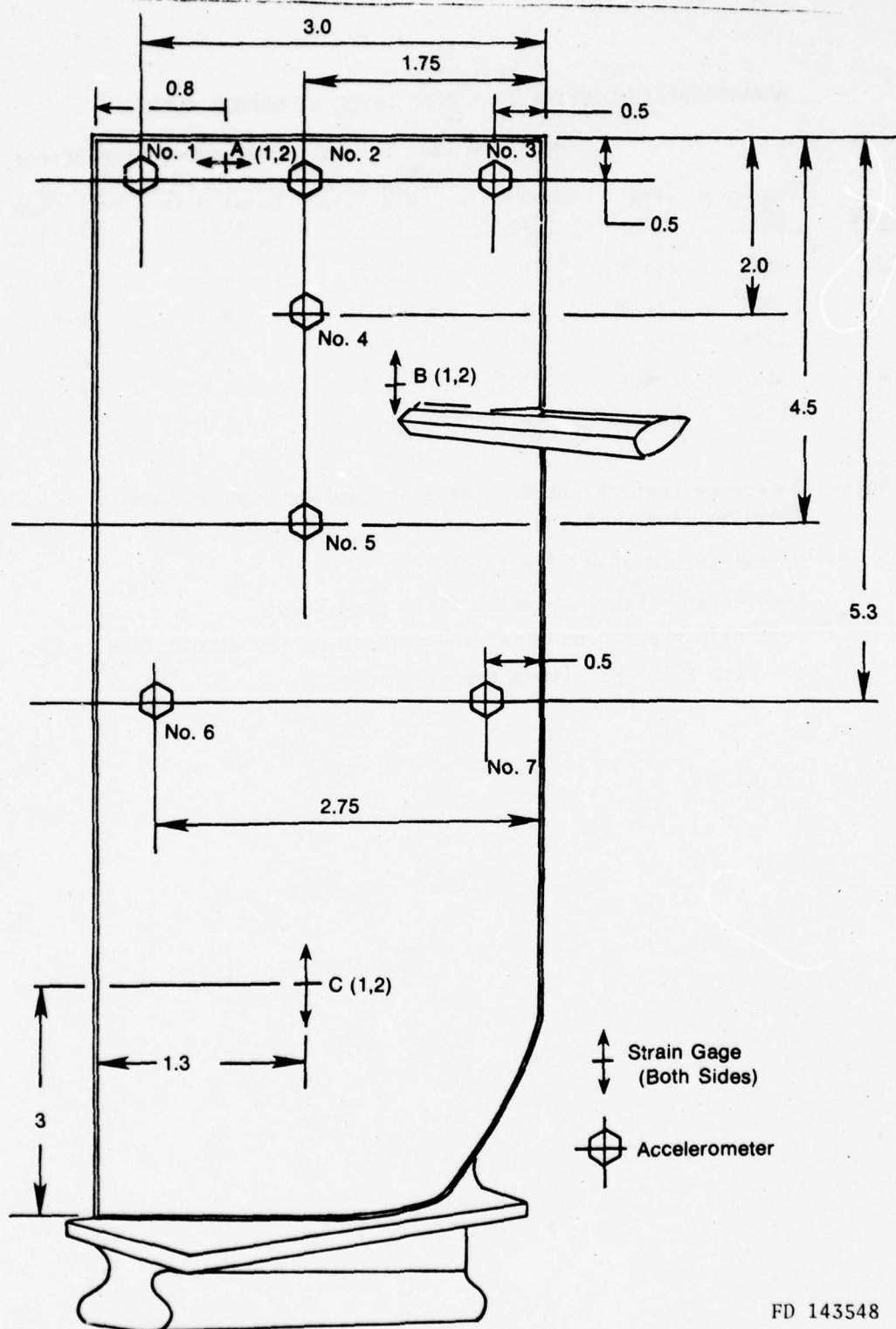
2. Final Test Phase

During the testing of a single blade mode, the shroud interface slips locally at a given excitation level. The region of local shroud interface slippage increases with increased dynamic loading until the entire shroud interface slides or slips across the restraint fixture. Local slip occurs when the local elastic shear force exceeds the friction force. Given the normal load distribution along the shroud interface, the magnitude of the local friction force can be calculated. The blade normal mode analysis with a ring shroud boundary condition provides modal elastic shear forces at the shroud interface and the modal stress distribution in the blade. The analysis indicated that stress levels in the blade, adjacent to the leading edge of the shroud, are sensitive to the blade deformed shape. Thus, the stress levels at this location

on the blade indicate the mode shape and relative load levels on the blade. Strain gages were applied to the blade to calibrate stress during the testing. The sensitive airfoil location near the shroud (gage "B") is shown in Figure 14.

During the tests, a 234-lb load was used to represent the normal load during the fully restrained shroud condition. The titanium shroud was flame sprayed with a carbide wear surface. The shroud face was in contact with a Waspaloy test fixture. A coefficient of friction of 0.4 was used for this combination of materials. Thus the total available friction force at the shroud interface and the distribution along the interface were calculated.

Microscopic slip occurs when the local elastic shear force is equal to or greater than the local friction force. Gross slip occurs when the total elastic force exceeds the total friction force. Using the modal stress and modal shear forces from the ring shroud normal mode analysis, the value of blade stress at which slip occurs was calculated. Table 2 shows the calculated values of stress level at the gage with the maximum value of stress and gage "B" (Figure 14) on the blade for which local slip and full slip of the shroud would occur. The calculated values of slip for the first two modes compared well to those measured in the laboratory testing.



FD 143548

Figure 14. Location of Blade Instrumentation

TABLE 2.
ANALYTICAL PREDICTION OF STRESS LEVEL AT SHROUD SLIP

| Mode | Frequency (Hz) | Type Mode | Amplitude Peak Stress (0-Peak) | | Reference Gage Stress (0-Peak) | |
|------|-------------------|--------------|-----------------------------------|--------------------|-----------------------------------|--------------------|
| | | | Local Slip (ksi) | Full Slip (ksi) | Local Slip (ksi) | Full Slip (ksi) |
| 1 | 351 | 1st B | 5.3 | 15.2 | 5.3 | 15.2 |
| 2 | 994 | 1st T | 1.2 | 14.3 | 0.5 | 6.5 |
| 3 | 1378 | 2nd B | 1.6 | 7.8 | 0.4 | 2.0 |
| 4 | 1537 | Compl | 1.2 | 7.1 | 0.8 | 4.7 |
| 5 | 1859 | Compl | 0.7 | 9.5 | 0.2 | 2.5 |

Note: Reference Gage "B" Blade Stress at Leading Edge of Shroud
(Figures 11 and 14)

Normal shroud load, $P = 234 \text{ lb}$

Local slip = Level at which first grid slips

Full slip = Based on total shear force on the shroud face

$E = 17.8 \times 10^6 \text{ psi}$ (room temperature)

SECTION V

TASK IV

EXPERIMENTAL TESTING

A. GENERAL

Initially, three YF100(I) trailing-edge-shroud blades were tested without instrumentation to determine their natural frequencies and correlate the findings with those of the NASTRAN analysis (Task II). A single fan blade (Serial Number CB3183) was then selected for further testing with and without instrumentation and under varied shroud load conditions.

B. TESTING PROCESS

1. Initial Fan Blade Testing

Initial testing of three YF100(I) trailing-edge-shroud blades was without the addition of strain gages or accelerometers. The first five natural frequencies were found for the blades with both unrestrained and fully restrained shroud conditions. Table 3 presents a comparison between the natural frequencies predicted by the NASTRAN analysis (Task II) and the mean test values for the unrestrained shroud conditions. Table 4 shows the natural frequencies found during laboratory testing for the blade with the shrouds restrained. The analytical predictions from the NASTRAN analysis for the ring shroud are also given in Table 4. A comparison of the test data with the analytical prediction of natural frequency shows good agreement.

TABLE 3.
ANALYTICAL VS TEST NATURAL FREQUENCY
FOR BLADE WITH UNRESTRAINED SHROUD

| | Mode | Mean Test Freq. (Hz) ¹ | NASTRAN Freq. (Hz) |
|---|---------------|--------------------------------------|-----------------------|
| 1 | 1st Bending | 104 | 102 |
| 2 | 2nd Bending | 323 | 306 |
| 3 | 1st Torsion | 569 | 613 |
| 4 | Complex Plate | 711 | 680 |
| 5 | Complex Plate | 1182 | 1227 |

1. Mean value of three blades tested.

TABLE 4.
ANALYTICAL VS TEST NATURAL FREQUENCY
FOR BLADE WITH RESTRAINED SHROUD¹

| | Mode | Mean Test Freq. ² (Hz) | NASTRAN Freq. ³ (Hz) |
|---|-------------|--------------------------------------|------------------------------------|
| 1 | 1st Bending | 376 | 351 |
| 2 | 1st Torsion | 1009 | 994 |
| 3 | 2nd Bending | 1311 | 1378 |
| 4 | Complex | 1550 | 1537 |
| 5 | Complex | 1923 | 1859 |

1. Normal load applied to shrouds P = 234 lb

2. Mean value of three blades tested

3. Ring shroud analysis

2. Initial Testing Phase of Single Fan Blade

a. Natural Frequency Testing

Based on the initial blade testing, a single fan blade (Serial Number CB3183) was selected for all further testing. To determine the repeatability of the blade testing, the blade was frequency retested six times with the shrouds restrained. The test consisted of installing the blade in the test fixture with a shroud load of 234 lb. The first three natural frequencies of the blade were determined using a low level of excitation. The shroud load was released and the blade removed from the fixture. The blade was reinstalled in the test fixture and the shroud load reapplied. The results of the first natural frequency showed a variance from the mean test value between +0.5% and -0.6%; the second frequency varied by $\pm 0.6\%$; and the third mode frequency varied by +0.3% and -0.6%.

The natural frequencies of the blade were then analytically determined with and without instrumentation. The fan blade weight without instrumentation was 452.2 grams. It increased to 458 grams with instrumentation. The calculated natural frequency decreased by 0.6% from the blade frequency before the addition of instrumentation, and was therefore considered an insignificant variation. This was confirmed by laboratory tests in which the natural frequencies of the instrumented and non-instrumented blade for both the restrained and unrestrained shroud conditions were measured. For the unrestrained shroud condition, the frequencies of the blade before and after the addition of instrumentation to the airfoil are shown in Table 5. The variation in frequency was between 0 and $1\frac{1}{2}\%$ for the first four modes.

TABLE 5.
UNRESTRAINED SHROUD BLADE TEST RESULTS

| Mode | Frequency (Hz) | | Delta Frequency |
|------|---------------------------|------------------------|--------------------|
| | Without Accelerometers | With Accelerometers | |
| 1 | 105 | 105 | 0 |
| 2 | 329 | 325 | -4 |
| 3 | 570 | 566 | -4 |
| 4 | 713 | 702 | -11 |

A second series of tests were performed on the blade with the shrouds fully restrained. A preload of 234 lb was applied to the shroud interfaces and the frequencies of the first four modes of the blade were again experimentally determined before and after the addition of instrumentation to the blade. The results are shown in Table 6.

The final testing of the blade primarily investigated shroud slippage in the first mode, which is the first bending mode. This mode showed a change of 0.7% in blade frequency during testing due to the instrumentation. Thus the effect of the added mass on the test results was considered negligible.

TABLE 6.
RESTRAINED SHROUD BLADE TEST RESULTS

| Mode | Natural Frequency (Hz) | | Delta Frequency |
|------|--------------------------|-----------------------|--------------------|
| | Without Accelerometer | With Accelerometer | |
| 1 | 387 | 384 | -3 |
| 2 | 1003 | 1001 | -2 |
| 3 | 1270 | 1234 | -36 |
| 4 | 1574 | 1578 | +4 |

b. Excitation Level - Blade Shroud Slippage Analysis

The first two modes of the blade with restrained shrouds were investigated to experimentally determine the level of input excitation at which the blade shrouds began to slip. The blade was restrained in the test fixture and the shroud interface load of 234 lb was applied. The

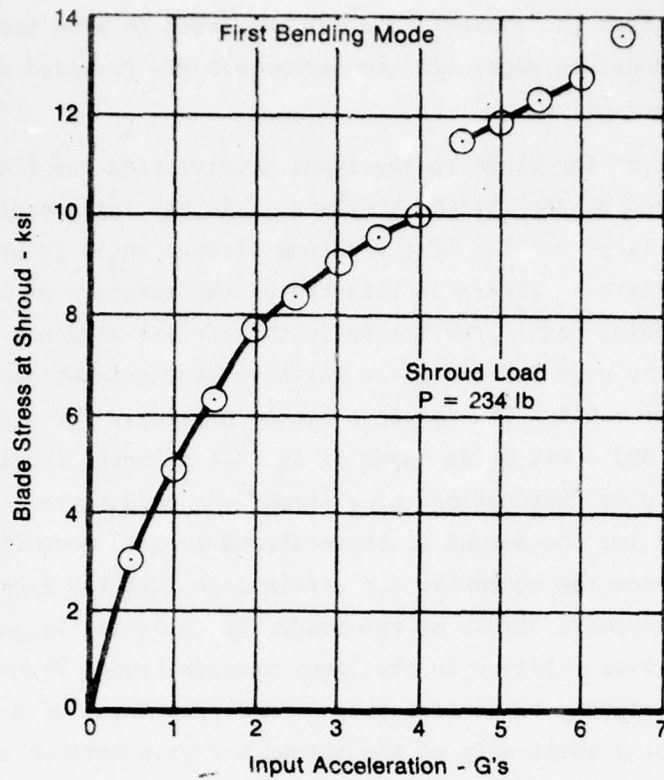
input excitation from the shaker table was increased in even increments. The output of the strain gages and accelerometers was recorded at each level of input excitation.

The response of the blade to the input acceleration was linear until local slip occurred at the shroud interfaces. As the input excitation was increased, a large portion of the shroud slipped until gross slippage of the shroud occurred. Figure 15 illustrates the response of the blade in the first bending mode. The stress in the airfoil adjacent to the shroud, recorded by gage "B" was given relative to the input acceleration of the shaker table. The response became nonlinear for stress levels between 4 and 5 ksi or an input of 1g. At a stress level of 10 ksi, gross slip or "ratcheting" of a shroud was encountered. The test was repeated for the second or above-shroud-torsion mode (Figure 16). For the torsion mode the chordwise tip strain gage gave the highest response. The chordwise stress at the blade tip, measured by gage "A" (Figure 14), is given relative to the input acceleration. Figure 16 shows the blade response to be linear up to a stress level of 0.6 ksi. The test data showed local slip of the shroud occurred between stress levels of 0.6 ksi and 1.0 ksi at the blade tip. As the input excitation was increased above 1.6 g's, the blade shroud interface "ratchets" across the shroud restraint test fixture.

The initial slip of the shroud interface was analytically predicted by the NASTRAN finite element model (Table 2) to occur at an airfoil stress of 5.3 ksi adjacent to the shroud for the first mode. The second mode was predicted to reach initial shroud slip at an airfoil tip chordwise stress level of 1.2 ksi. These stress levels were calculated using a coefficient of friction equal to 0.4. The laboratory test data indicate that initial slip of the shroud occurs at stress levels between 4 to 5 ksi for the first mode and 0.6 ksi for the torsional mode.

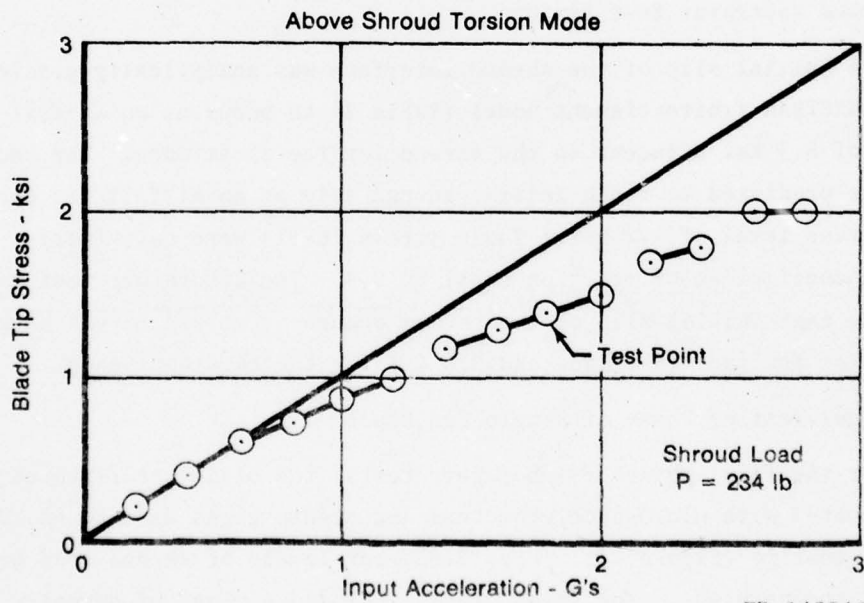
3. Final Testing Phase of Single Fan Blade

For the final phase of laboratory tests, the blade was fixtured and instrumented with micro-accelerometers and strain gages as done in the initial testing (Figure 14). Five different levels of shroud load were applied to the blade. The shroud loads included a range of normal



FD 143545

Figure 15. Stress/Excitation in First Mode



FD 143546

Figure 16. Stress/Excitation in Torsion Mode

load from 100 to 400 lb. A reference level of 234 lb, which represents the load level developed during normal flight operation of the blade, was included in the range of test conditions. At each magnitude of shroud load the blade was excited at resonance for at least three different levels of input acceleration.

At the beginning of the test, shroud faces and load platens were cleaned and degreased. The shroud loading platens were brought into contact with the shroud faces. The screw mechanism was advanced until the desired shroud load level was obtained. The magnitude of force was indicated by a meter attached to a load cell. In applying the shroud load, the blade was carefully located centrally in the test apparatus and uniformly loaded to ensure repeatability.

At each level of input excitation for a given shroud load, the magnitude and phase of each accelerometer was recorded. The frequencies at peak response and stress levels of the strain gages were recorded. Preliminary testing showed the response of accelerometer number one (Figure 14) was representative of test conditions with reference to the other accelerometers for the shrouded blade response. Therefore, to determine the system damping, a plot of the number one accelerometer response as a function of frequency was generated at each level of input acceleration. Using the half power power technique,* system damping was determined.

Figures 15 and 16, which were generated during preliminary testing of the blade, show that for relatively low levels of input excitation the response of the blade becomes nonlinear. This indicates that local or microslip of the shroud face occurred at low levels of excitation. The point of gross slip of the shroud is indicated by a loss of relief of the applied shroud load. As the input excitation was increased, and as the point of gross slip was approached, the shroud load began to diminish until the point of almost complete loss was reached.

*Harris, C., C. Crede, Shock and Vibration Handbook McGraw Hill Book Company, 1976, pp. 2-15.

Examination of the shroud load platens after the shroud load was relieved showed material transfer from the shroud face to the load platens. Reinstalling the shroud load after slip occurred allowed a higher level of shear load to be developed at the interface. This resulted in a change in the magnitude of the response for a given set of test conditions, shroud load, and input excitation. To ensure repeatability of the tests once gross slip (loss of the shroud load) occurred, the blade was removed from the test apparatus and the load platens re-polished to remove any material transferred to them. By careful control of the shroud interface and load platen surfaces, repeatable test data were obtained for the blade up to the condition of gross slip.

The use of low levels of normal shroud loads in conjunction with high levels of excitation results in gross slippage of the shrouds. As explained, once gross slippage occurred, the normal shroud loads applied by the test fixture were relieved. Also associated with a freely slipping shroud is a change in shroud face boundary conditions due to material transfer between the shroud and the test fixture. Due to these factors it was not possible to obtain repeatable test data for a blade with freely slipping shrouds.

Figure 15 presents data gathered in the preliminary testing of the blade in the first bending mode. This curve shows a discontinuity of data at 5 g's of input excitation. Further testing of the blade showed that a loss of shroud load indicative of gross slip occurred at this level of input excitation.

The blade was tested in the first bending mode with a shroud load of 234 lb. Figure 17 shows the phase relation between the motion at the blade root and the blade tip as indicated by accelerometers numbers one and six. Analytical calculations showed that for a locked shroud, high shroud load and low input excitation during the test, the motion of the blade occurred primarily above the shroud. The motion below the shroud was of very low magnitude and 90-deg out of phase relative to the tip deflections. (See Figure 4, Section III for the analytically generated modal displacements for the first bending mode with a locked shroud.) For a slipping shroud the motion below the shroud is more significant

in magnitude and is in phase with the tip motion. (See Figure 6, Section III for the analytically predicted modal displacement for a blade with a slipping shroud.)

Figure 17 shows that as the magnitude of input excitation approaches the point at which the shroud load is relieved, the tip motion and root motion become closer in phase indicating a shift from a ring shroud to a slipping shroud condition. Only a small variation in resonant frequency was observed in the laboratory testing as the input excitation was increased to the point of shroud load loss as depicted in Figure 18.

The amount of system damping for the shrouded fan blade was determined experimentally. Preliminary testing demonstrated that accelerometers at the tip were most responsive. A graph was generated of the accelerometer output magnitude as a sweep of the excitation frequency through resonance. By applying the half power point technique to the curve, the system damping was determined.

The blade was initially tested in the first torsion mode. The magnitude of damping for the first torsion mode, as shown in Figure 19, was found to be insensitive to the magnitude of shroud load or input level of excitation. The system damping given as a percent of critical damping was found to vary between 0.13 to 0.15% over a range of input excitation from 1 to 6 g's.

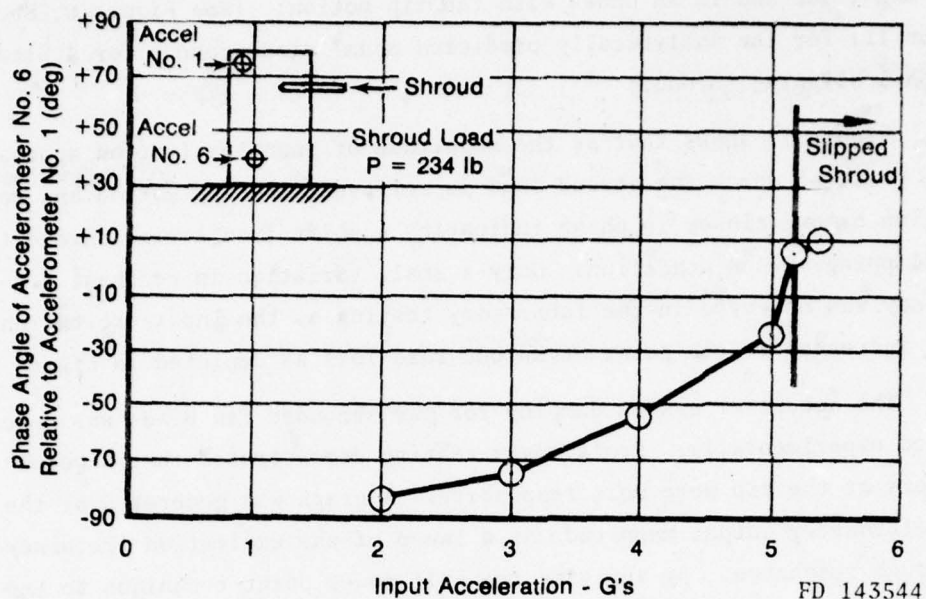


Figure 17. Phase Relation Between Tip to Root Accelerometers in First Bending Mode versus Input Excitation Level

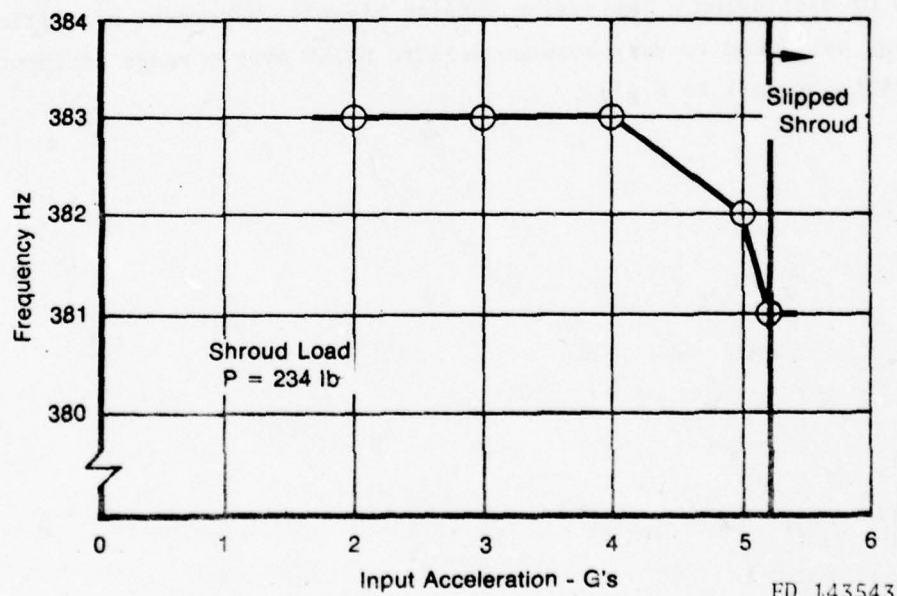


Figure 18. Frequency versus Input Excitation Level for First Bending Mode

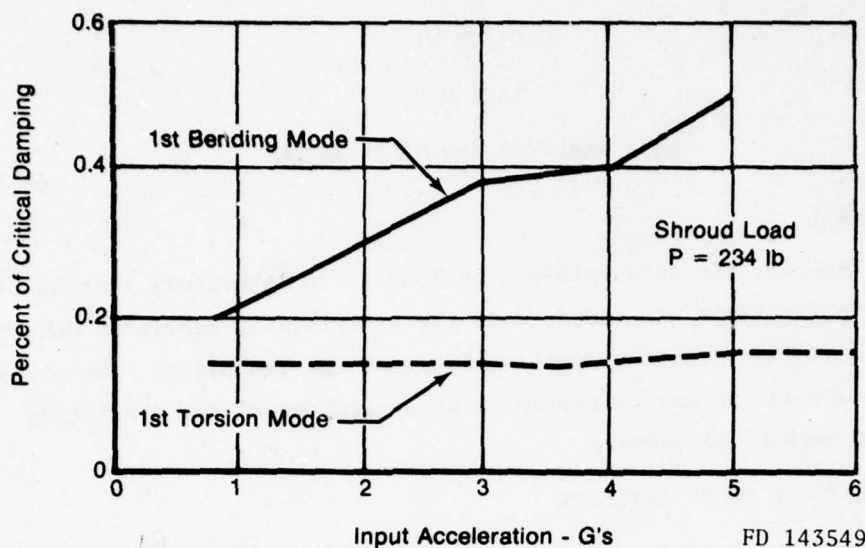


Figure 19. Percent of Critical Damping versus Input Excitation for a Constant Shroud Load

Testing the blade in the first bending mode showed a more significant effect on damping caused by changing the input excitation (Figure 19). The data in Figure 19 were for a constant level of shroud load. The effect on damping caused by changing the shroud load is illustrated in Figure 20.

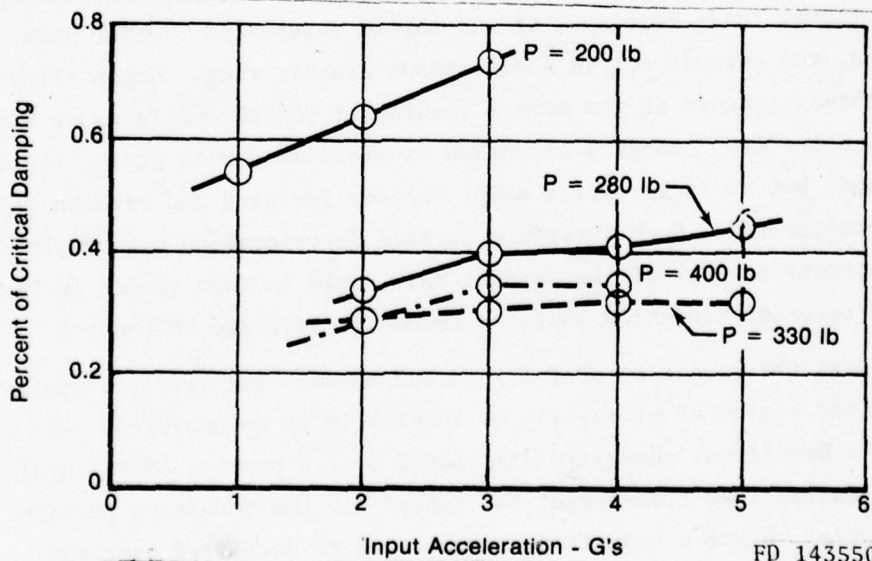


Figure 20. Percent of Critical Damping versus Input Excitation for First Bending Mode

SECTION VI

TASK V

DATA ANALYSES AND CORRELATION

A. GENERAL

In Task VI, the data obtained in Task IV in laboratory testing of the single fan blade was compared to the analytically generated data by using the NASTRAN finite element analysis of the fan blade. The purpose of this correlation was to refine an analytical model for predicting fan blade mechanical damping.

B. ANALYTICAL MODEL ANALYSIS

1. General Background

The shrouds of a shrouded fan blade form a segmented ring when the blades are assembled into the disk assembly. At operational speed, the blade centrifugal loading causes the blade to untwist or rotate about a radial axis. The untwisting of the blades forces the shroud faces into intimate contact with the adjacent shroud blade. Thus the shroud contact or normal load is a function of the initial assembly fit of the shrouds and the rotational speed of the fan assembly during operation. At a high normal shroud load, the shrouds are fully locked together by the frictional loads developed at the shroud interfaces. Under this condition, the shrouds act as a continuous elastic ring. Gross slipping of the shrouds occurs at low normal loading of the shroud faces or high excitation levels. Energy dissipation is associated with gross slip of the shroud, but at large cyclic slip, serious fretting and erosion effects may be encountered. Such interface surface deterioration may result in fatigue cracks or wear of the shroud; this could in turn result in highly stressed resonant vibration that the shroud is intended to control.

Between the condition of fully locked shrouds and freely slipping shrouds, the region of micro-slip or local slip is encountered. For the micro-slip condition, energy is dissipated over a portion of the cycle with an elastic load transfer at the shroud for the remaining portion of the cycle. Since a nonuniform normal load is developed over the shroud, the frictional shear force will also vary across the shroud face.

Therefore, during a blade vibration cycle, some points along the interface will be transferring load elastically as other points slip.

2. Blade Shroud Stick-Slip Analysis

In order to investigate the shear loads along the shroud interface, the simple spring/mass system illustrated in Figure 21 was used to investigate the relation between blade motion and the shear loads at the shroud. The blade is represented by the mass, M , which undergoes the simple harmonic motion denoted by the symbol (δ) . The normal load at the shroud is denoted as " N_i "; relative motion at the shroud face, or slip, is represented by the symbol " X ". At a high value of normal shroud load, the shroud does not slip, $X=0$. For this condition the shear load at the shroud is determined from the following expression which indicates a linear elastic load

$$F_L = K_i \delta_b$$

Where:

F_L = linear shear load at shroud

K_i = shroud stiffness

δ_b = blade motion.

During slip ($X \neq 0$), the shear load is equal to the frictional load

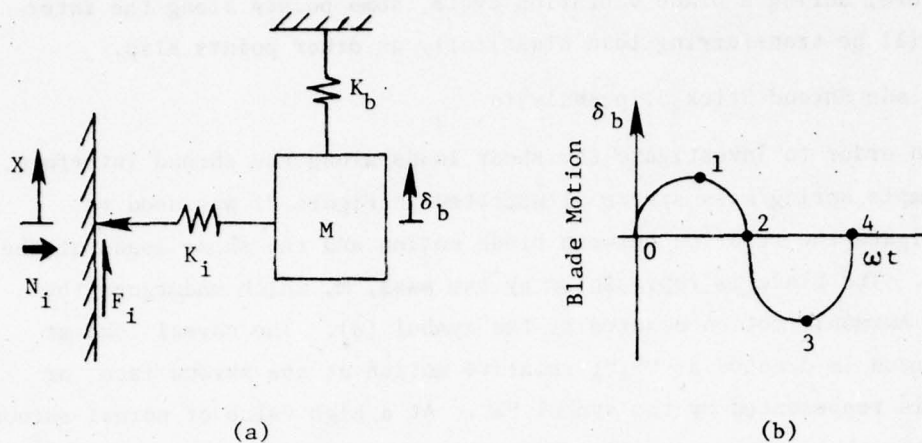
$$F_S = \mu N_i$$

Where:

F_S = shear load at shroud during slip

μ = coefficient of friction

N_i = load normal to the shroud face.



M = Mass
 K_i = Stiffness of Shroud
 δ_b = Blade Motion
 N_i = Normal Load at Point "i"
 F_i = Interface Shear Load at Point "i"
 x = Slip Motion at Shroud Interface
 K_b = Stiffness of Blade

Figure 21. Simple One-Degree-of-Freedom Model

The elastic shear load is equal to the frictional shear load at the instant before slip. By equating the expression for elastic load to the friction force expression, the amount of the blade motion required to cause slip at the shroud can be calculated at the start of slip:

$$\begin{aligned}
 F_L &= F_s \\
 K_i \delta &= \mu N_i \\
 \therefore \delta_{\text{slip}} &= \frac{\mu N_i}{K_i} = \Delta
 \end{aligned}$$

Figure 22 illustrates the relation between blade motion and slip at the shroud for the simple model depicted by Figure 21. The numbers in Figure 22 relate to the position in the displacement plot of Figure 21. The motion of the blade starts at point "0" and is elastic until slip

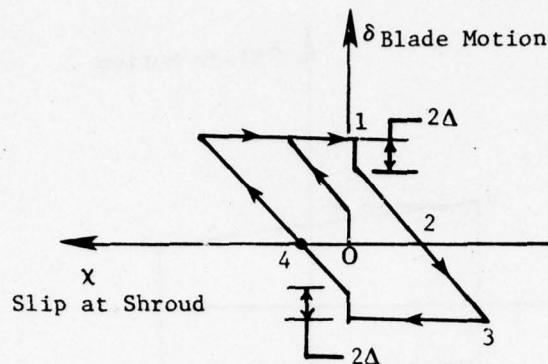
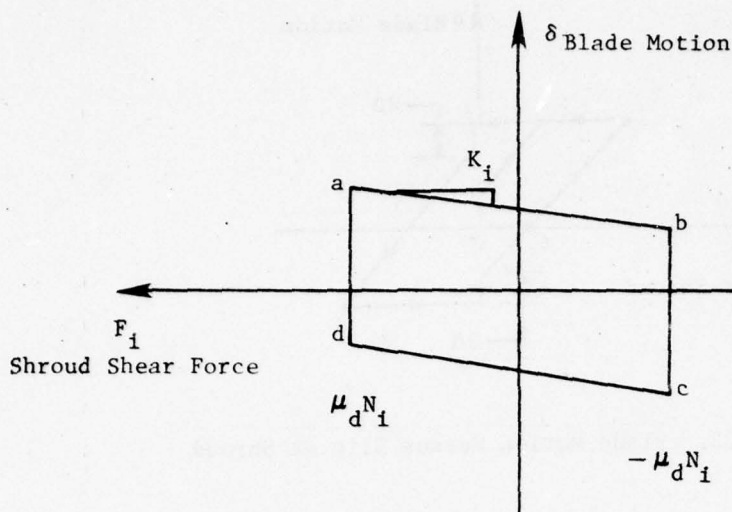


Figure 22. Blade Motion Versus Slip at Shroud

occurs as illustrated in Figure 22. Motion of the mass continues with slip until the maximum displacement is reached. At point "1", the shroud spring " K_i " is loaded to the magnitude caused by the blade motion " Δ ". As the motion of mass "M" continues at point "1", the spring " K_i " is first unloaded and then reloaded as the motion changes direction. Therefore, the shroud force is elastic for a blade motion equal to 2Δ , as illustrated in Figure 22. The shroud slips as the mass moves through point "2" to the maximum negative displacement, point "3". Slip motion stops as the blade reverses direction. The blade must displace " 2Δ " for slip to reoccur. The cycle continues with the mass moving around the curve through point "4" back to point "1" to continue a new cycle.

The shear force at the shroud face expressed as a function of the blade motion is illustrated in Figure 23. The shroud force is elastic along line "ab". Referring to Figure 22, this motion is equal to the blade moving from point "1" through " 2Δ ". After the blade has moved through the distance " 2Δ ", slip occurs at the shroud face. The shear load at the shroud face is shown schematically in Figure 23 to be equal to the coefficient of friction times the normal load. This is illustrated by line "bc" (Figure 23). The load is again elastic from point c to point d. This is equivalent to the motion of " 2Δ " on the lower portion of Figure 22, after which slip occurs limiting the load to the frictional value.



F_i = Shear Force at Shroud
 δ = Blade Motion
 μ = Coefficient of Friction
 N_i = Normal Load at Shroud
 K_i = Shroud Stiffness

Figure 23. Blade Motion Versus Shear Force at Shroud Face

The effect of increasing the normal shroud load is illustrated in Figure 24. As the normal shroud load is increased, the shroud undergoes a transition from a slipping shroud to a fully locked shroud. Increasing the normal load from (N) to (N') causes the amount of the cycle during which the shroud remains stuck to increase from 2Δ to $2\Delta'$. Figure 24 also shows that the load remains elastic for a greater amount of blade motion as the normal load is increased. The limiting value of the normal load is the point at which 2Δ is equal to the full range of blade motion from zero to the maximum. At this value of normal load, no slip would occur during the complete cycle. That is, $X=0$ over the entire cycle. When this condition is reached, the shroud shear force versus the blade motion (in a diagram) degenerates to a single line; the slope of this line is equal to the shroud stiffness.

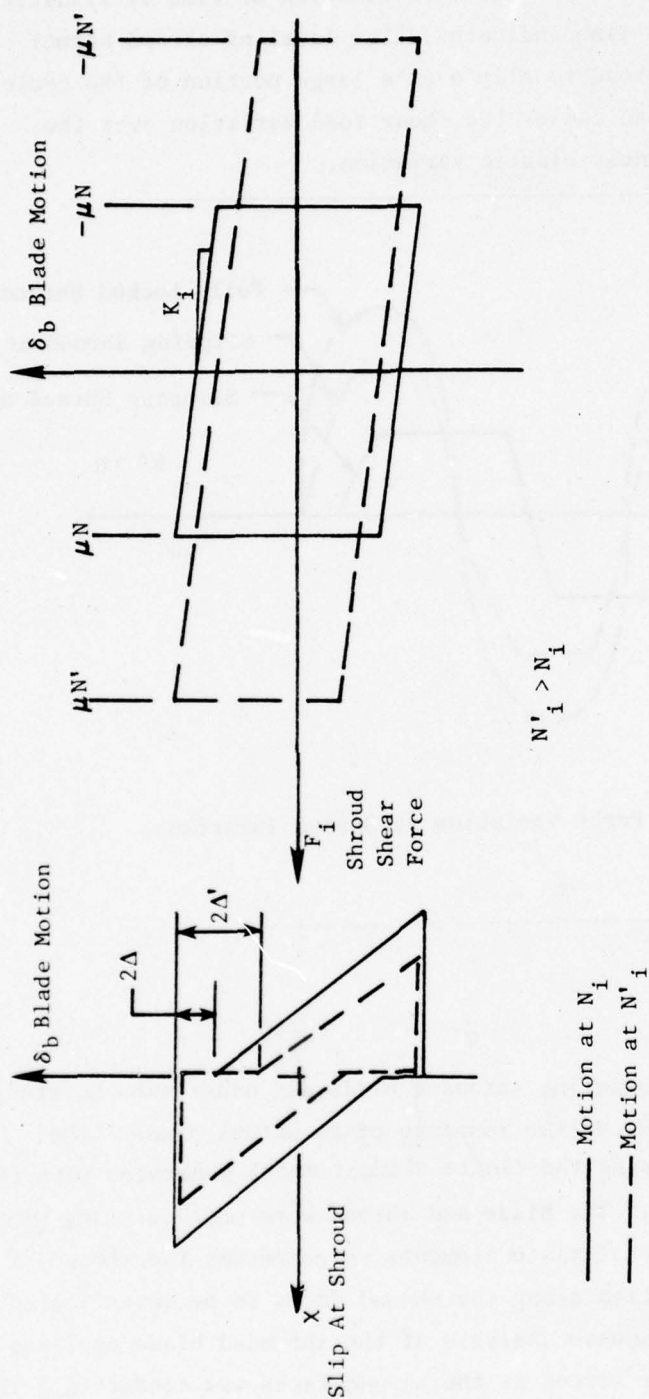


Figure 24. Transition from Slipping Shroud to Fully Locked Shroud

The shroud interface shear load as a function of time is illustrated in Figure 25. The solid line indicates a low level of shroud normal load which allows the shroud to slip over a large portion of the cycle. Increasing the normal load causes the shear load variation over the cycle to approach the linear elastic variation.

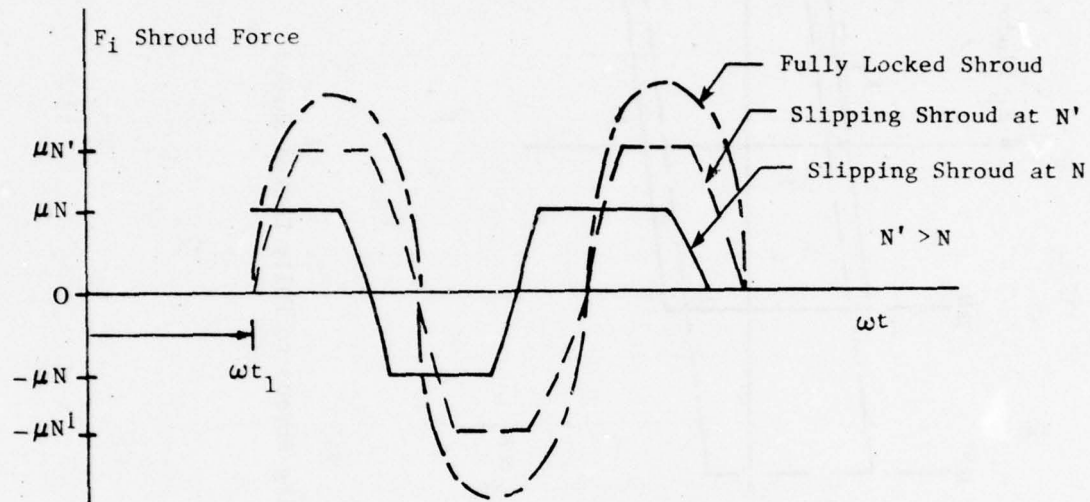


Figure 25. Force Variation at Shroud Interface

3. NASTRAN Analysis

a. General

The analysis of an existing shrouded blade was undertaken to study the effect of shroud loads on the response of an actual blade. The analysis was conducted using the finite element model generated with the NASTRAN computer program. The blade and shroud were modeled using plate finite elements. The use of plate elements to represent the shroud allows the load distribution along the shroud faces to be investigated. A steady-state forced response analysis of the shrouded blade applying a base excitation and shear forces at the shroud faces was conducted. The results from the analysis were compared to laboratory test data generated in Task IV.

The shear load at the shroud face (as explained in the beginning of this section) is dependent on the load normal to the shroud face, the stiffness of the shroud, and the blade motion. This results in a nonlinear problem. An iterative solution to the response problem is required.

A reference point on the blade-shroud junction was used to monitor blade motion. Starting the analysis with an assumed blade motion, the shroud loads were calculated. The estimated shroud load was applied to the forced response model and a base excitation to determine the blade response. The motion determined from the analysis was compared to the initial estimate of displacement. When the new displacement was equal to the estimate, the solution was accepted. When the new value of displacement differed from the original value, the new value was used to recalculate the shroud loads. This procedure was repeated until a solution was reached, as illustrated in Figure 26.

b. Prediction of Slip

The distribution of normal load along each of the shroud faces was determined with a NASTRAN static finite element analysis of the shrouded blade. (The determination of the normal load distribution was discussed in Section IV. The distribution of the normal shroud loads are shown in Figure 13.)

Knowing the normal load distribution, the Coulomb frictional shear forces along the shroud may be calculated for a given coefficient of friction and magnitude of normal load.

The elastic shear loads developed at the shrouds for a given excitation were determined from a forced response analysis of the blade with the shrouds fixed. By comparing the elastic shear loads at the shroud with the frictional shear loads, the relation between the normal load required to prevent slip and the input excitation was determined.

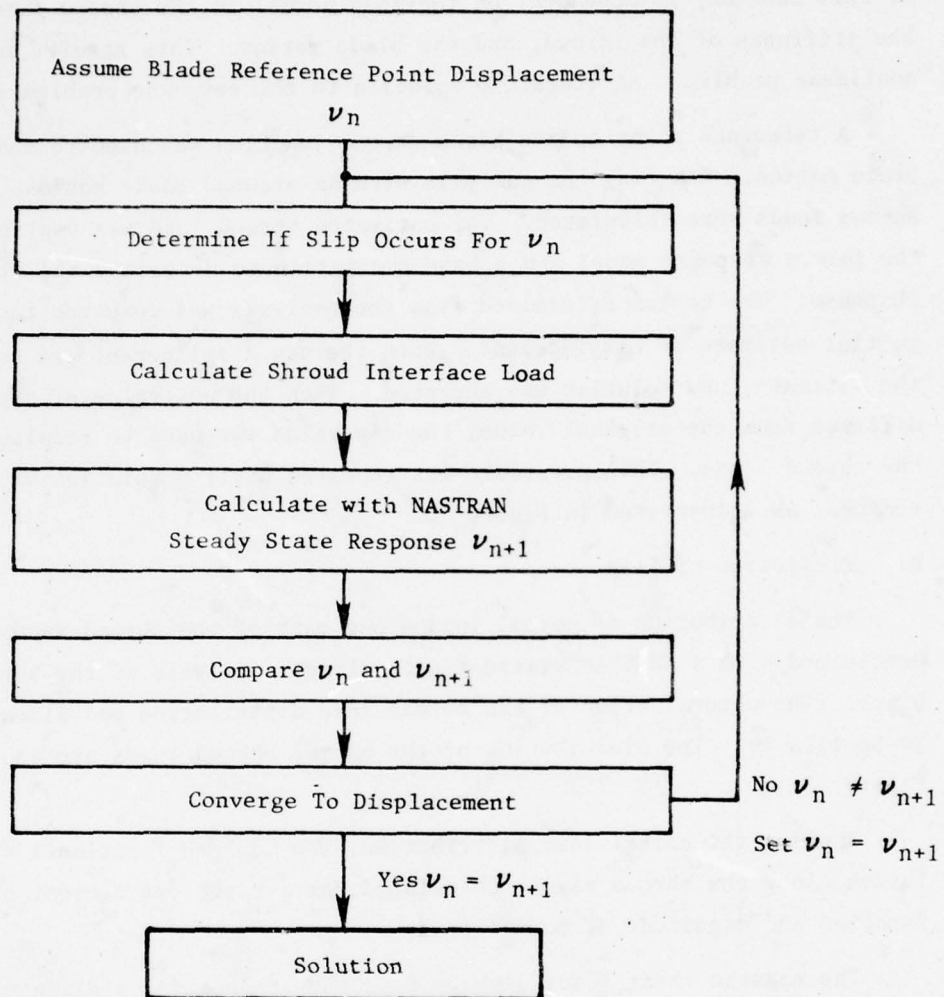


Figure 26. Analysis Procedure Flow Chart

Figure 27 illustrates the relation between the normal shroud load and input excitation for the YF100(I) first-stage blade with a trailing edge shroud. This graph is based on a coefficient of friction equal to four tenths. Figure 27 also includes the range of normal shroud loads used during the laboratory testing of the blade. It illustrates that conditions ranging from fully locked shrouds to slipping shrouds were encountered

during blade testing. The effect of the coefficient of friction on the shroud slip is illustrated in Figure 28. This curve represents the blade subjected to a 2g excitation.

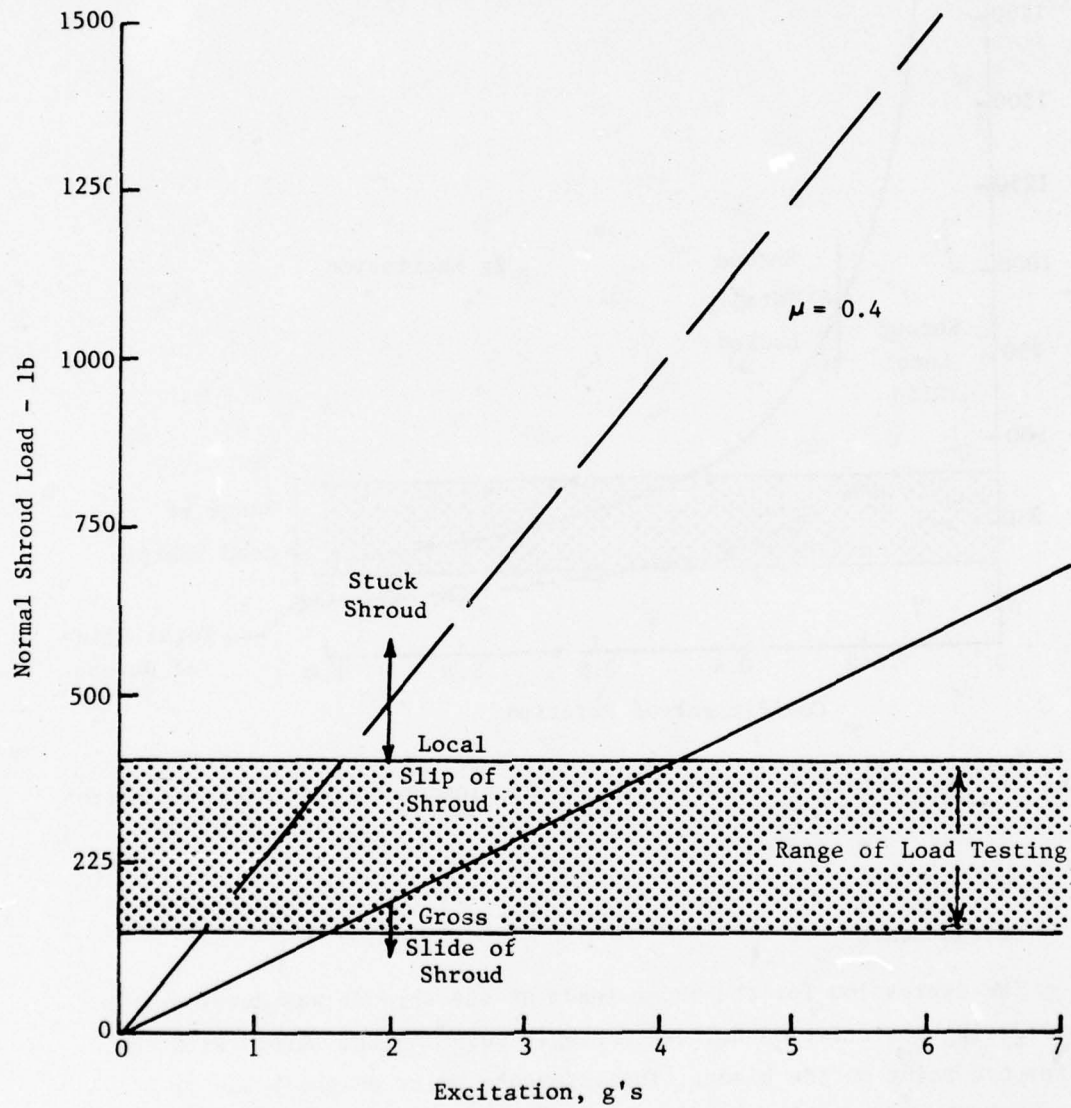


Figure 27. Analytical Prediction of the Effect of Normal Shroud Load on Shroud Interface Motion

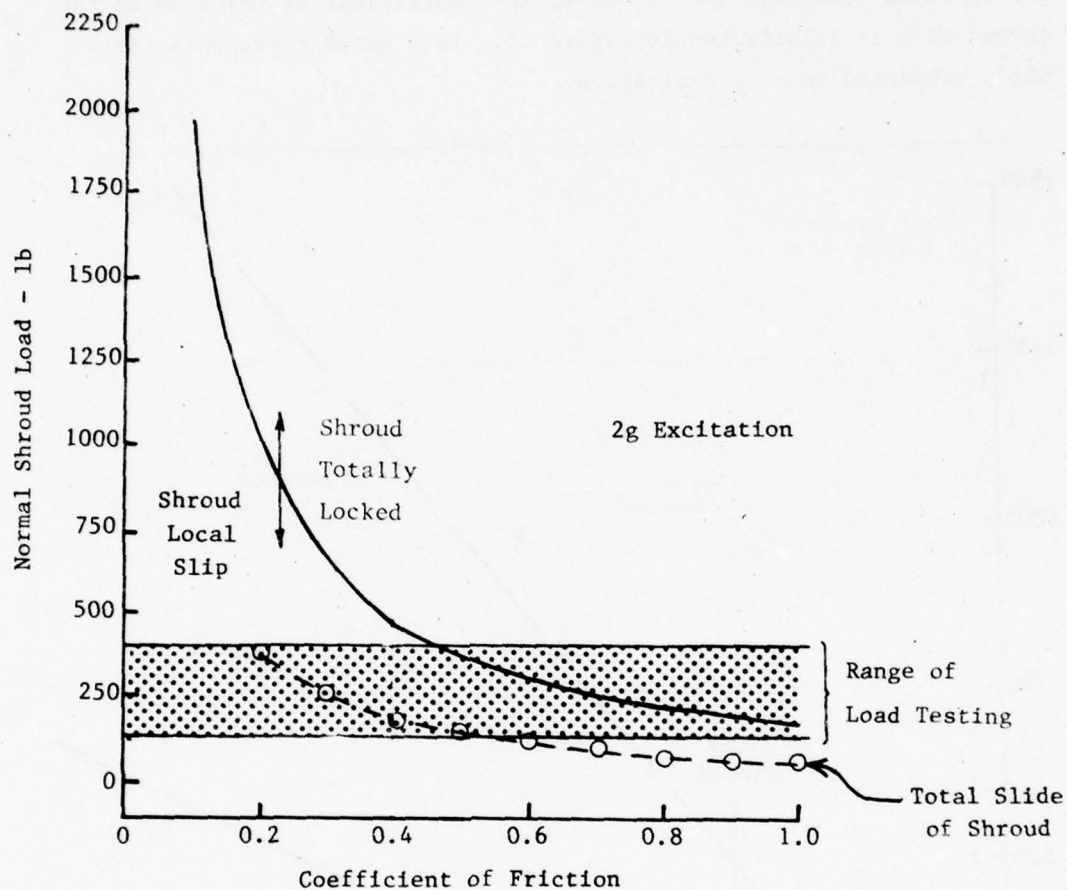


Figure 28. The Effect of Coefficient of Friction on Shroud Interface Motion

c. Shroud Loads

The expression for the shear loads at the shrouds was developed by considering the relation between a single point on the shroud with the reference point on the blade. The reference point on the blade is a point at the center of the blade shroud junction. Figure 29 illustrates the general form of the load over a cycle. The load is expressed by a discontinuous function over the complete cycle. For the steady-state response of the blade the cycle is arbitrarily started at time t_1 . The

shroud is "stuck" over the portion of the cycle denoted by the time interval t^* . The four expressions used to describe the shroud load over the cycle are:

$$\begin{aligned} F_R^I &= -\mu N - KU [\cos(\omega t - \psi) - 1] & \psi \leq \omega t \leq \psi + \omega t^* \\ F_R^{II} &= \mu N & \psi + \omega t^* \leq \omega t \leq \psi + \pi \\ F_R^{III} &= \mu N - KU [\cos(\omega t - \psi) + 1] & \psi + \pi \leq \omega t \leq \psi + \pi + \omega t^* \\ F_R^{IV} &= -\mu N & \psi + \pi + \omega t^* \leq \omega t \leq \psi + 2\pi \end{aligned}$$

Where:

$$\psi = \omega t_1$$

$$\mu = \text{coefficient of friction}$$

$$N = \text{normal shroud load at point "i"}$$

$$K = \text{stiffness of shroud point "i" relative to the blade reference point}$$

$$\omega = \text{frequency}$$

$$t = \text{time}$$

$$U = \text{blade reference point motion.}$$

By equating the expressions for the shroud load at the point which an elastic load ends and slip starts, an expression for ωt^* may be defined at

$$\omega t = \psi + \omega t^*$$

$$F_R^I = F_R^{II}$$

$$-\mu N - KU [\cos(\omega t^*) - 1] = \mu N$$

$$\omega t^* = \cos^{-1} \left[1 - \frac{2\mu N}{KU} \right].$$

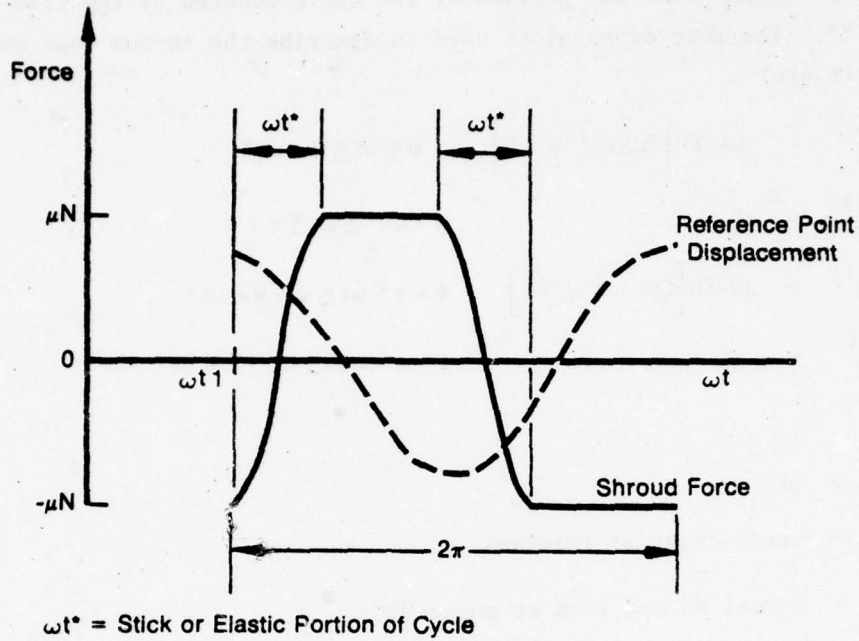


Figure 29. Local Shroud Force for Stick-Slip Condition

As the ratio $\frac{\mu N}{KU}$ (the ratio of Coulomb friction load to elastic load) approaches unity the magnitude of ωt^* approaches π . Thus at values of the ratio $\frac{\mu N}{KU} \geq 1$, the shear load at the shroud point under study is elastic. As the ratio is reduced from unity, slip occurs over an increasing portion of the cycle.

In order to use the shroud load expression in a forced response analysis, the general discontinuous expression is represented by a Fourier Series.

Where:

$$f_t = \frac{a_0}{2} + \sum_{n=1}^{\infty} (A_n \cos n\omega t + b_n \sin n\omega t).$$

It can be shown that only odd terms exist and that:

$$a_0 = 0$$

$$a_1 = -\frac{2D}{\pi} \sin(\omega t^*) + \frac{2A}{\pi} \sin(\omega t^*) - \frac{B}{\pi} \left\{ \omega t^* + \frac{1}{2} \sin 2\omega t^* \right\}$$

$$a_3 = -\frac{2D}{3\pi} \sin(3\omega t^*) + \frac{2A}{3\pi} \sin(3\omega t^*) - \frac{B}{2\pi} \left\{ \sin 2\omega t^* \right\} - \frac{B}{4\pi} \left\{ \sin 4\omega t^* \right\}$$

$$\begin{aligned}
a_5 &= -\frac{2D}{5\pi}\sin(5\omega t^*) + \frac{2A}{5\pi}\sin 5\omega t^* - \frac{B}{4\pi}\sin 4\omega t^* - \frac{B}{6\pi}\sin 6\omega t^* \\
b_1 &= \frac{2D}{\pi}\left[1+\cos\omega t^*\right] + \frac{2A}{\pi}\left[1-\cos\omega t^*\right] - \frac{B}{\pi}\sin^2\omega t^* \\
b_3 &= \frac{2D}{3\pi}\left[1+\cos 3\omega t^*\right] + \frac{2A}{3\pi}\left[1-\cos 3\omega t^*\right] + \frac{B}{2\pi}\left[\cos(2\omega t^*)-1\right] \\
&\quad + \frac{B}{4\pi}\left[\cos(4\omega t^*)-1\right] \\
b_5 &= \frac{2D}{5\pi}\left[1+\cos 5\omega t^*\right] + \frac{2A}{5\pi}\left[1-\cos 5\omega t^*\right] + \frac{B}{4\pi}\left[\cos(4\omega t^*)-1\right] \\
&\quad + \frac{B}{6\pi}\left[\cos(6\omega t^*)-1\right]
\end{aligned}$$

Where:

$$\begin{aligned}
A &= \left[KU - \mu N\right] \\
B &= KU \\
D &= \mu N \\
\omega t^* &= \cos^{-1}\left[1 - \frac{2\mu N}{KU}\right]
\end{aligned}$$

The Fourier Series expression evaluated at a ratio of $\mu N/KU$ equal to unity degenerates to the simple elastic harmonic expression as shown in Figure 30. Figure 31 illustrates the original shroud load curve evaluated at a ratio of $\mu N/KU = \frac{1}{2}$. This represents the condition of slip over 50% of the cycle. Shown relative to the original curve are the results of evaluating the Fourier Series using the first three harmonics for this condition and also the results of using only the first harmonic in the load evaluation. The result of using the first three harmonics in defining the load matches the original curve very closely. The use of only the first harmonic results in a small variation between the loading curves. The extreme conditions with slip over 80% of the cycle is illustrated in Figure 32. This figure shows that the use of only the first terms in the Fourier Series load definition closely matches the original curve. The two curves deviate by 8%. As the amount of slip over the cycle decreases, that is as the ratio of $\mu N/KU$ approaches unity, the deviation diminishes between the original curve and the load definition based on only the first harmonic from the Fourier Series definition of the load. At the point of no slip the expressions match. The analysis of the blade was conducted using the first harmonic from the Fourier Series expression of the shroud load.

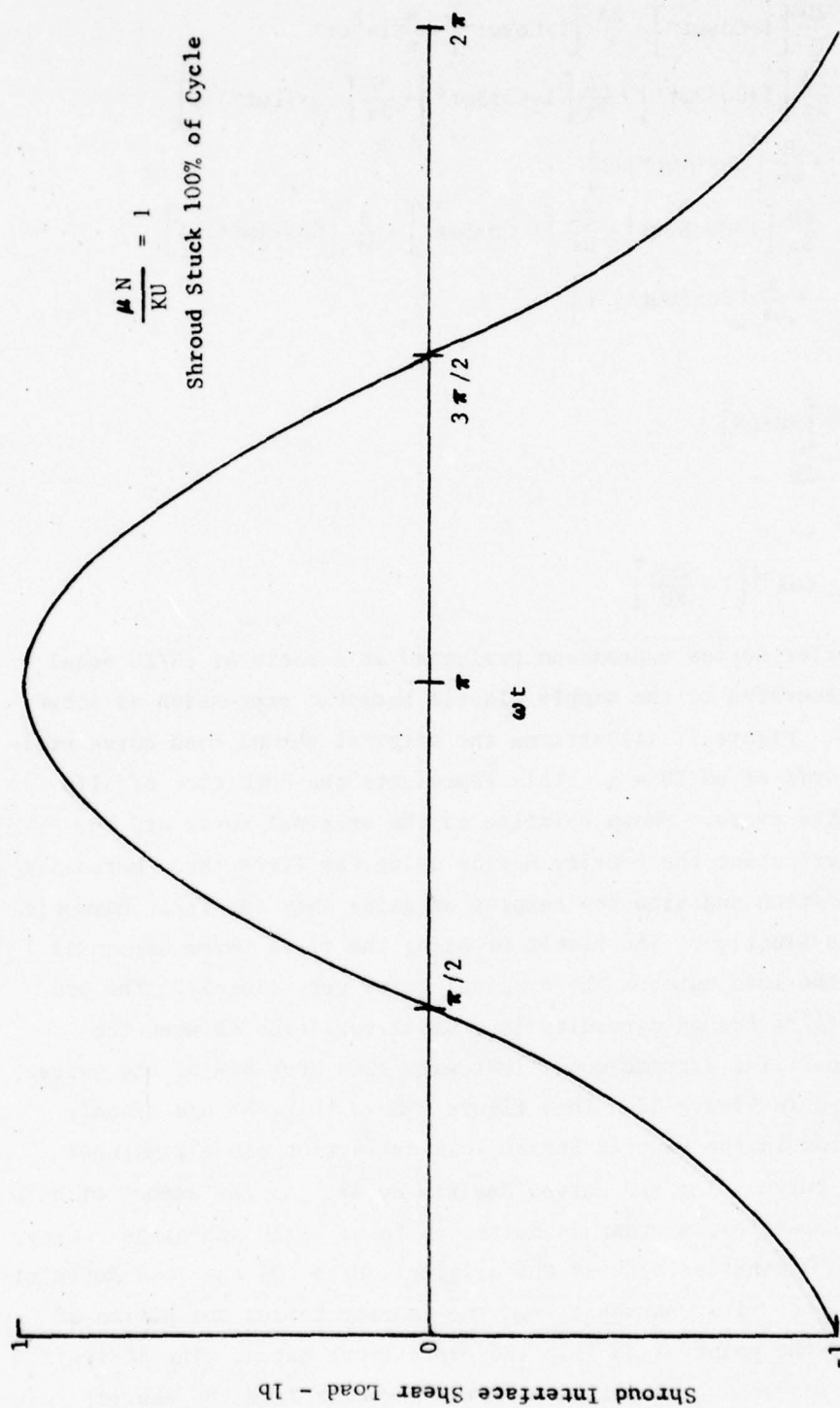


Figure 30. Analytical Representation of Shroud Interface Load Over a Cycle Where $\mu N/KU = 1$

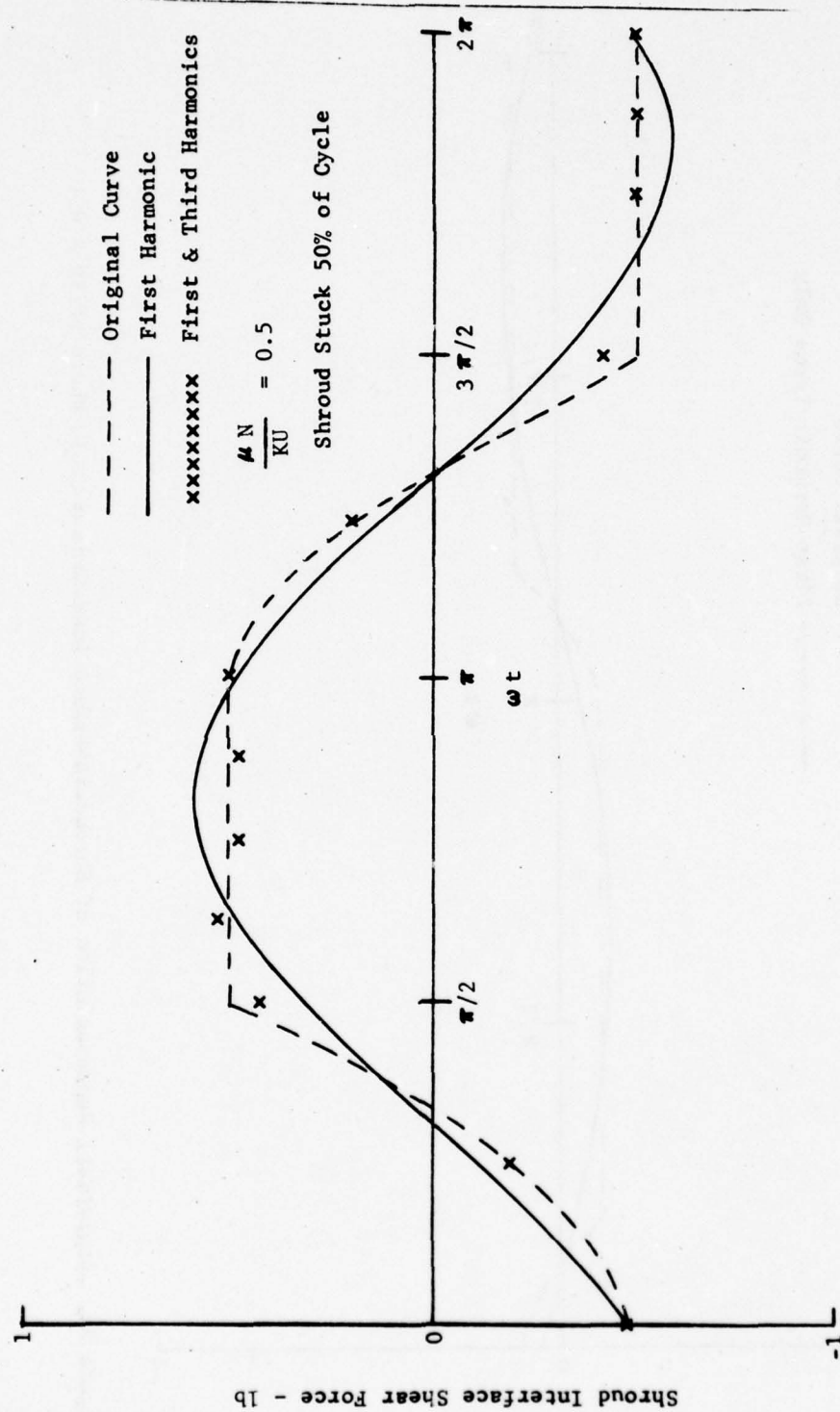


Figure 31. Analytical Representation of Shroud Interface Load Over a Cycle Where $\mu N/KU = 0.5$

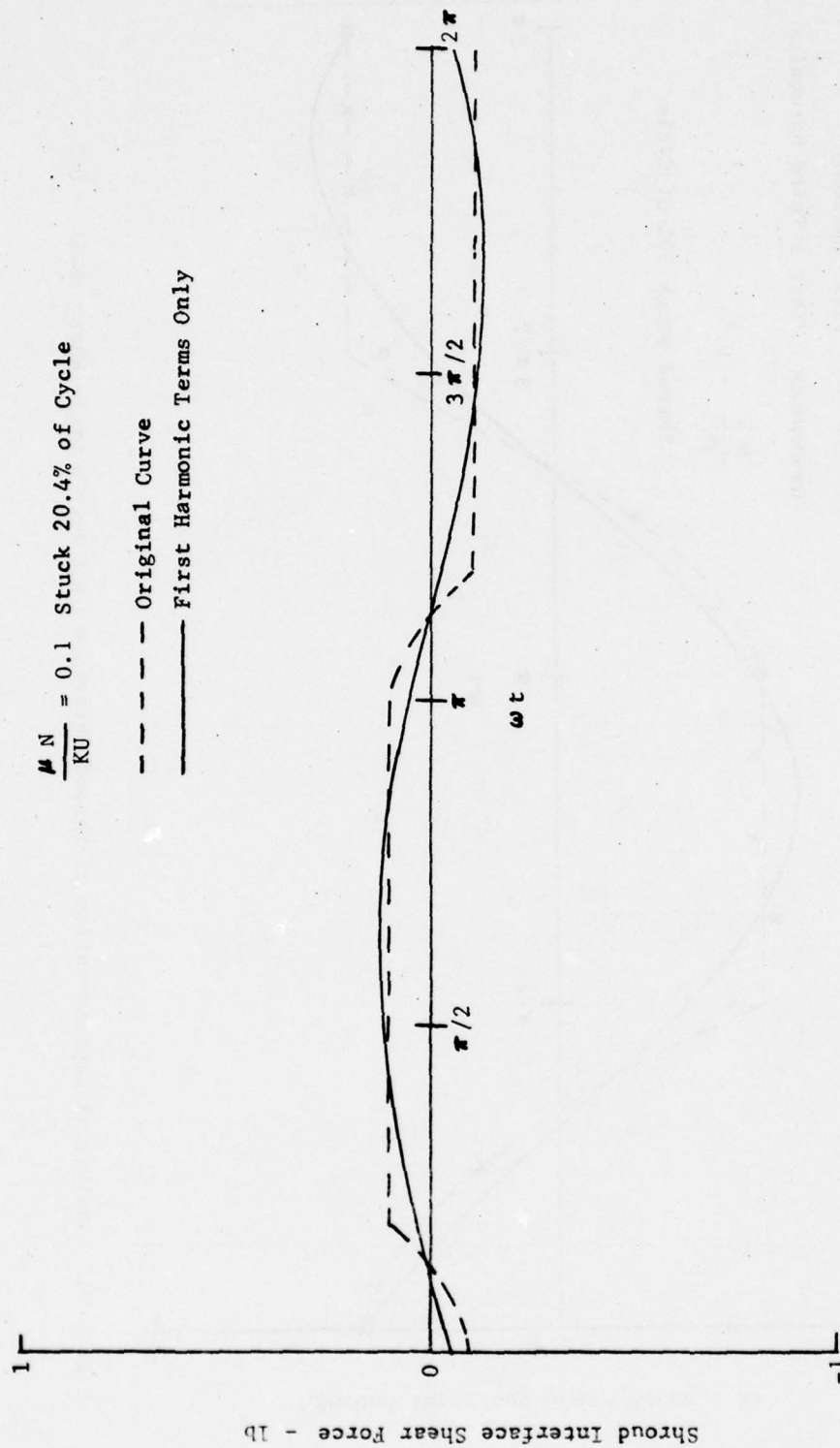


Figure 32. Analytical Representation of Shroud Interface Load Over a Cycle Where $\mu N/KU = 0.1$

d. Blade Analysis

A forced response steady-state analysis was conducted using the NASTRAN finite element computer program. (The mathematical model used for the analysis was shown in Figure 2.) The blade was subjected to a base excitation at the root attachment and the shear loads were prescribed along the shroud faces. The shroud shear loads, both in-plane and out of the shroud plane, were determined using the first harmonic of the Fourier Series expression for the shroud loads. Five grid points along each of the shroud faces were defined in the model which allowed the shear load variation to be included in the analysis. Since the shroud loads are a function of the blade motion, an iterative solution was required to solve the blade response problem (Figure 26). The rate of convergence of the iteration scheme is illustrated for two different analyses in Figure 33. The lower curve represents the blade in a micro-slip or stick-slip condition. The upper curve illustrates the solution converging to a blade with a stuck or fixed shroud.

The effect of changing the coefficient of friction on the solution is presented in Figure 28. For the case of $2g$'s base excitation, a shroud normal load of 234 lb, and the coefficient of friction equal to 0.8, Figure 28 predicts that the shrouds do not slip. The blade was analyzed under the above conditions first with the shrouds restrained from sliding and a second time with shroud shear loads calculated using a coefficient of friction equal to 0.8. Figure 33 shows that the iterative solution with a high coefficient of friction converges to the solution of the blade with fixed shrouds after five iterations. This agrees with the prediction of a non-slip response solution of Figure 28. Figure 33 also illustrates that with slip occurring, represented by the lower response curve, the energy dissipation of the shroud loading results in a lower tip response for the blade subjected to the same base excitation.

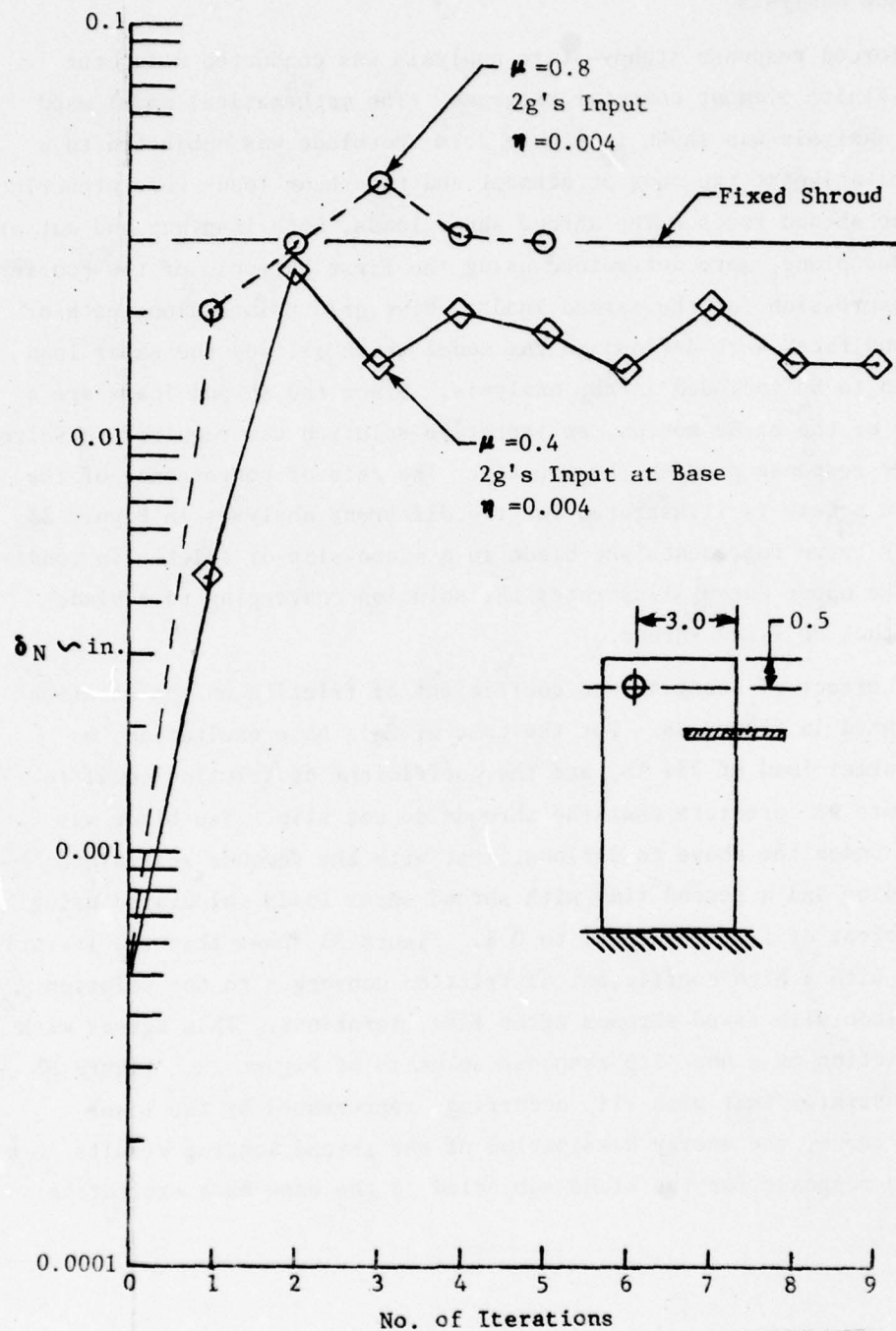


Figure 33. Analytical Predicted Normal Displacement at Blade Tip $\omega = 345 \text{ Hz}$, Normal Shroud Load: $N=234 \text{ lb}$

C. COMPARISON OF ANALYTICAL DATA TO TEST DATA

A comparison of analytical and test data generated for the blade under similar conditions shows good agreement, (Figure 34). The conditions illustrated are for the blade with local slip occurring during the cycle. The blade response for the other conditions tested are illustrated in Figure 35. The complete test results are presented in the appendix.

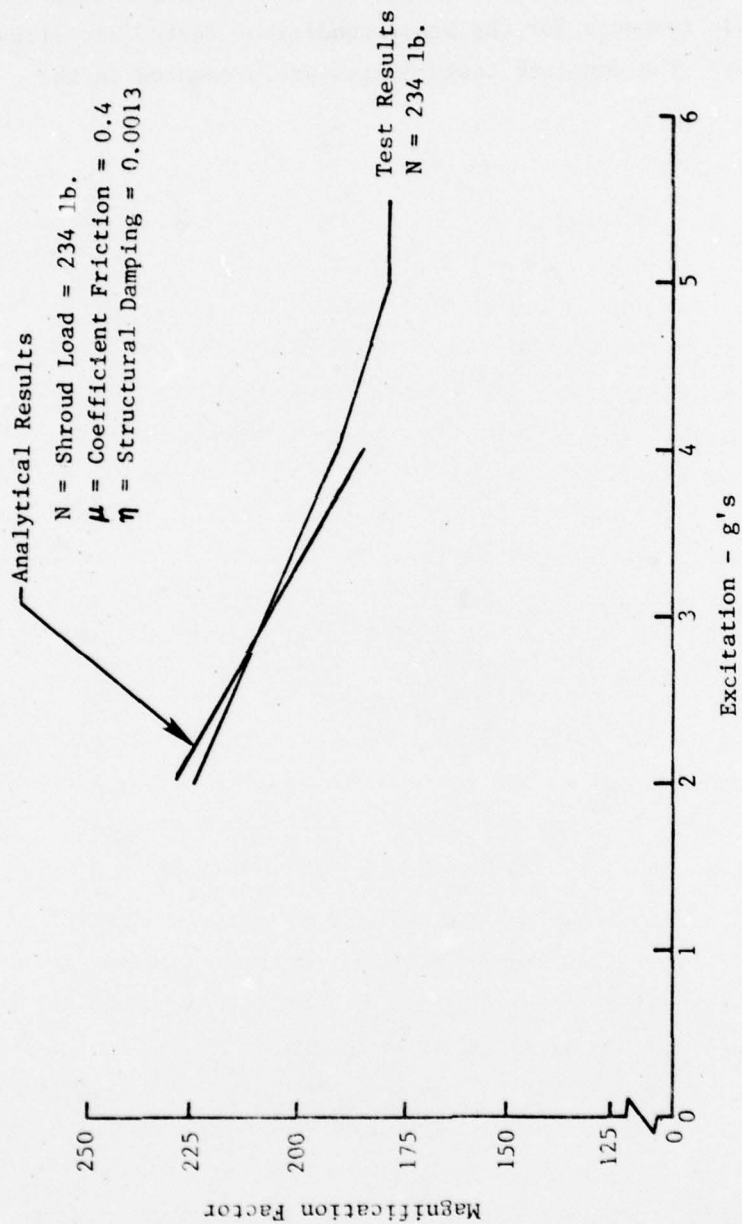


Figure 34. Analytical and Test Results Comparison of Blade Tip Response vs Input Excitation

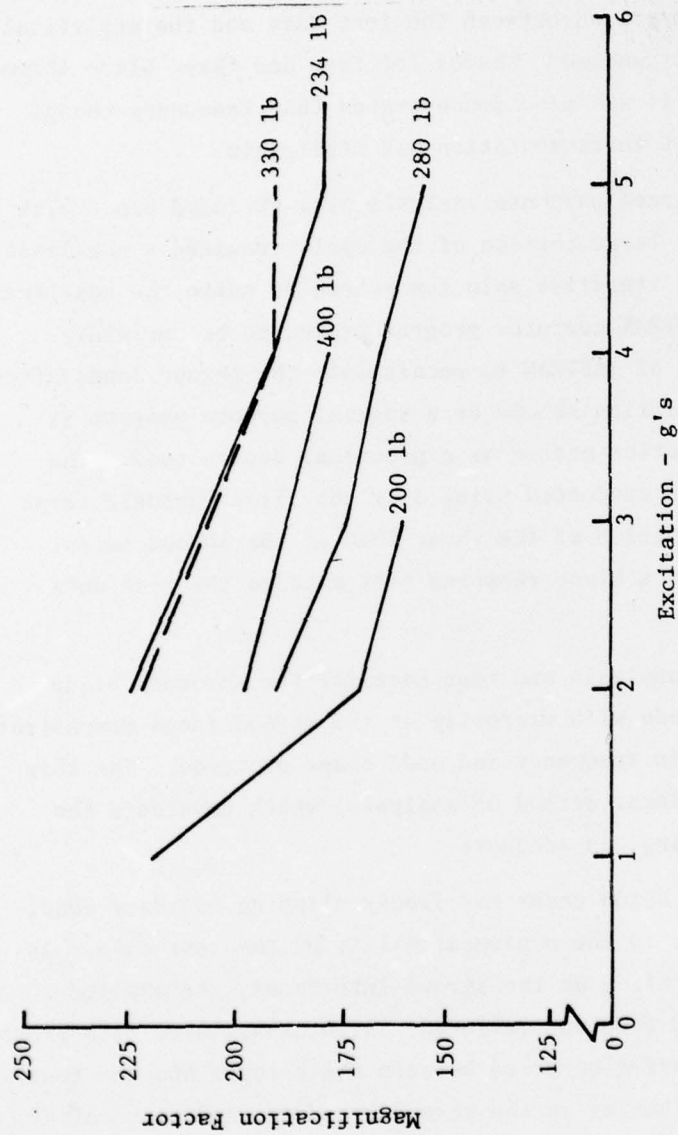


Figure 35. Blade Tip Response vs Input Excitation For Given Shroud Normal Loads During Testing

SECTION VII

CONCLUSIONS/RECOMMENDATIONS

Laboratory testing of the YF100(I) fan blade with a trailing edge shroud examined the full range of shroud boundary conditions from fixed to freely slipping. Comparison between the test data and the analytical prediction of frequencies and mode shapes for free and fixed blade shrouds showed good agreement. It was also demonstrated that frequency change caused by the presence of instrumentation was negligible.

The steady-state forced response analysis of a shrouded blade with shrouds that slip over a large portion of the cycle required a non-linear solution. The use of an iterative solution scheme to solve the non-linear problem based on the NASTRAN computer program proved to be unwieldy. An internal modification of NASTRAN to recalculate the shroud loads after each iteration in the solution scheme or a special purpose program is required to use this solution method as a practical design tool. The analysis of the blade was conducted using only the first harmonic terms of the mathematical definition of the shear load at the shroud faces. This analysis resulted in a blade response that matched the test data generated for the blade.

Comparisons of the analysis and test data for the shrouded blade vibrating in the first mode with microslip at the shroud faces demonstrated that only small changes in frequency and mode shape occurred. For this condition, the present linear method of analysis, which considers the shroud as a continuous ring, is adequate.

Analysis of the fan blade under the freely slipping boundary condition was inconclusive due to the nonrepeatability of the test data. As the fan blade started to slide at the shroud interfaces, the applied load normal to the shroud face was relieved. Also, associated with gross slipping, a material transfer occurred between the shrouds and the test fixture. The resultant changes in the shroud boundary conditions after gross slip had occurred negated test repeatability at the given shroud loads and input excitations. In order to evaluate this condition, a more sophisticated experimental approach would be required. A full stage of fan blades would have to be tested in a rotating environment with appropriate capability to modify shroud loads and measure response.

APPENDIX
TEST RESULTS

The test data generated during Task IV of the Fan Blade Damping Analysis Program is included in this section. Tables A1 through A5 present the stress output and accelerometer readings generated while testing the fan blade in the first bending mode with the shroud normal load held at 200 lb, 234 lb, 280 lb, 330 lb and 400 lb, respectively. The location of the strain gages and accelerometers was presented in Figure 14, Section IV. When the first mode is excited strain gage "B" is the only gage which yields a significant value. Therefore only the results from this strain gage appears in tables A1 through A5. The accelerometer output presented in the tables consists of the magnitude expressed in g's and the phase angle in degrees relative to the input excitation.

Figure A1 presents the bench test frequencies of the three blades used for the program and an indication of the mode shape of the blade. The tabular data are for blade Serial Number 3183.

Figures A2 through A6 illustrate the blade response of blade Serial Number 3183 as recorded by accelerometer number one. The curves present the tip response of the blade versus excitation frequency at different levels of input excitation for a fixed shroud normal load.

TABLE 7.
FAN BLADE TESTING IN FIRST BENDING MODE WITH A SHROUD LOAD = 200 lb

| Frequency (Hz) | Input Excitation | Accelerometer Output (g's) | | | | Stress Gage "B" (ksi) |
|-------------------|---------------------|----------------------------|-------------------------|-------------------------|------------------------|--------------------------|
| | | Gage No. 1 | Gage No. 3 | Gage No. 4 | Gage No. 6 | |
| 387.2 | 1g | 220 105 ^o | 120 105 ^o | 50 105 ^o | 0.2 5 ^o | |
| 386.6 | 2g | 340 95 ^o | 220 100 ^o | 92 120 ^o | 0.4 27 ^o | 4.6 |
| 385.9 | 3g | 480 100 ^o | 280 100 ^o | 105 100 ^o | 0.5 50 ^o | 5.9 |

TABLE 8.
FAN BLADE TESTING IN FIRST BENDING MODE WITH A SHROUD LOAD = 234 lb

| Frequency (Hz) | Input Excitation | Accelerometer Output (g's) | | | | Stress Gage "B" (ksi) |
|-------------------|---------------------|----------------------------|-------------------------|-------------------------|-------------------------|--------------------------|
| | | Gage No. 1 | Gage No. 3 | Gage No. 4 | Gage No. 6 | |
| 384.1 | 2g | 450 100 ^o | 250 140 ^o | 82 140 ^o | 0.3 15 ^o | 4.8/5.0 |
| 383.8 | 3g | 620 95 ^o | 360 98 ^o | 140 98 ^o | 0.3 20 ^o | 8.7/8.8 |
| 383.6 | 4g | 760 96 ^o | 430 105 ^o | 160 105 ^o | 0.5 40 ^o | 10.57/10.89 |
| 383.4 | 5g | 890 95 ^o | 500 90 ^o | 180 93 ^o | 0.6 70 ^o | 11.8/12.2 |
| 381 | 5.2g ¹ | 940 90 ^o | 520 90 ^o | 195 90 ^o | 1.0 105 ^o | 12.3/12.9 |
| 381 | 5.4g ² | 965 90 ^o | 520 90 ^o | 190 95 ^o | 1.2 100 ^o | 12.6/12.9 |

NOTE:

¹ Shroud Load starts being relieved

² Shroud Load relieved

TABLE 9.
FAN BLADE TESTING IN FIRST BENDING MODE WITH A SHROUD LOAD = 280 lb

| Frequency (Hz) | Input Excitation | Accelerometer Output (g's) | | | | Stress Gage "B" (ksi) |
|-------------------|---------------------|----------------------------|-------------|-------------|------------|--------------------------|
| | | Gage No. 1 | Gage No. 3 | Gage No. 4 | Gage No. 6 | |
| 384.9 | 2g | 380 100° | 230 100° | 90 110° | 0.2 15° | 5.5 |
| 384.4 | 3g | 520 100° | 300 100° | 110 106° | 0.3 45° | 7.7 |
| 384.1 | 4g | 660 100° | 480 100° | 140 100° | 0.4 30° | 9.6 |

TABLE 10.
SHROUD LOAD 330 lb

| Frequency (Hz) | Input Excitation | Accelerometer Output (g's) | | | | Stress Gage "B" (ksi) |
|-------------------|---------------------|----------------------------|-------------|-------------|-------------|--------------------------|
| | | Gage No. 1 | Gage No. 3 | Gage No. 4 | Gage No. 6 | |
| 385.9 | 2g | 445 90° | 260° 90° | 100 90° | 0.3 25° | 6.68 |
| 384.9 | 4g | 760 115° | 440 105° | 150 90° | 0.5 50° | 10.24 |
| 384.6 | 5g | 950 100° | 510 100° | 200 100° | 1.0 100° | 12.01 |
| | 6g | * | ~ | ~ | ~ | - |

*Shroud load relieved

TABLE 11.
FAN BLADE TESTING IN FIRST BENDING MODE WITH A SHROUD LOAD = 400 lb

| Frequency (Hz) | Input Excitation | Accelerometer Output (g's) | | | | Stress Gage "B" (ksi) |
|-------------------|---------------------|----------------------------|-------------------------|-------------------------|------------------------|--------------------------|
| | | Gage No. 1 | Gage No. 3 | Gage No. 4 | Gage No. 6 | |
| 385.9 | 2g | 395 105 ^o | 220 105 ^o | 91 105 ^o | 0.4 30 ^o | 7.75 |
| 385.5 | 3g | 560 100 ^o | 320 100 ^o | 120 100 ^o | 0.5 60 ^o | 7.93 |
| 385.3 | 4g | 710 100 ^o | 390 100 ^o | 160 98 ^o | 0.6 80 ^o | 9.85 |
| ~ | 5g | * | ~ | ~ | ~ | ~ |

*Shroud load relieved

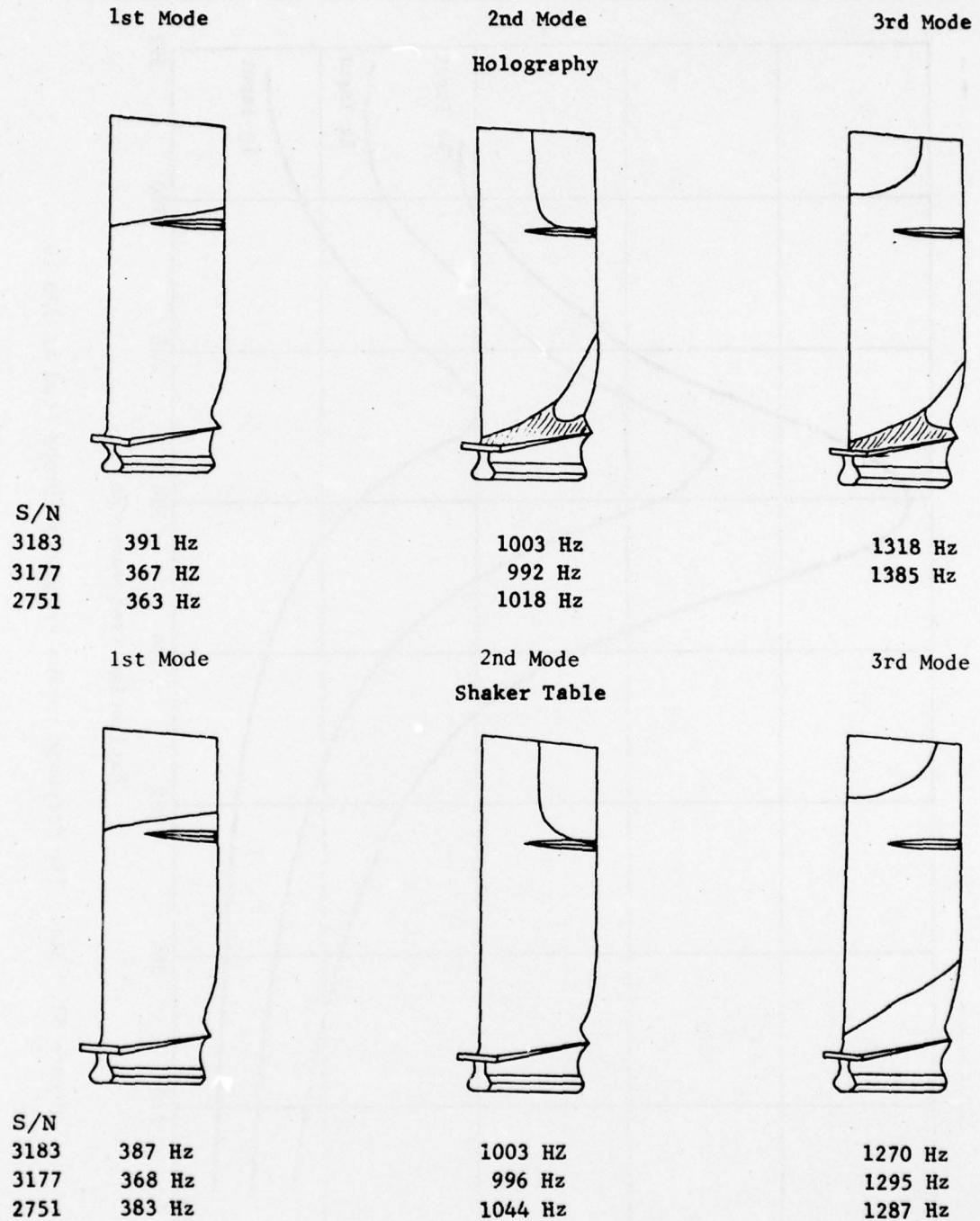


Figure 36. Blade Mode Shapes and Frequency from Bench Testing With Shrouds Restrained at 234 lb

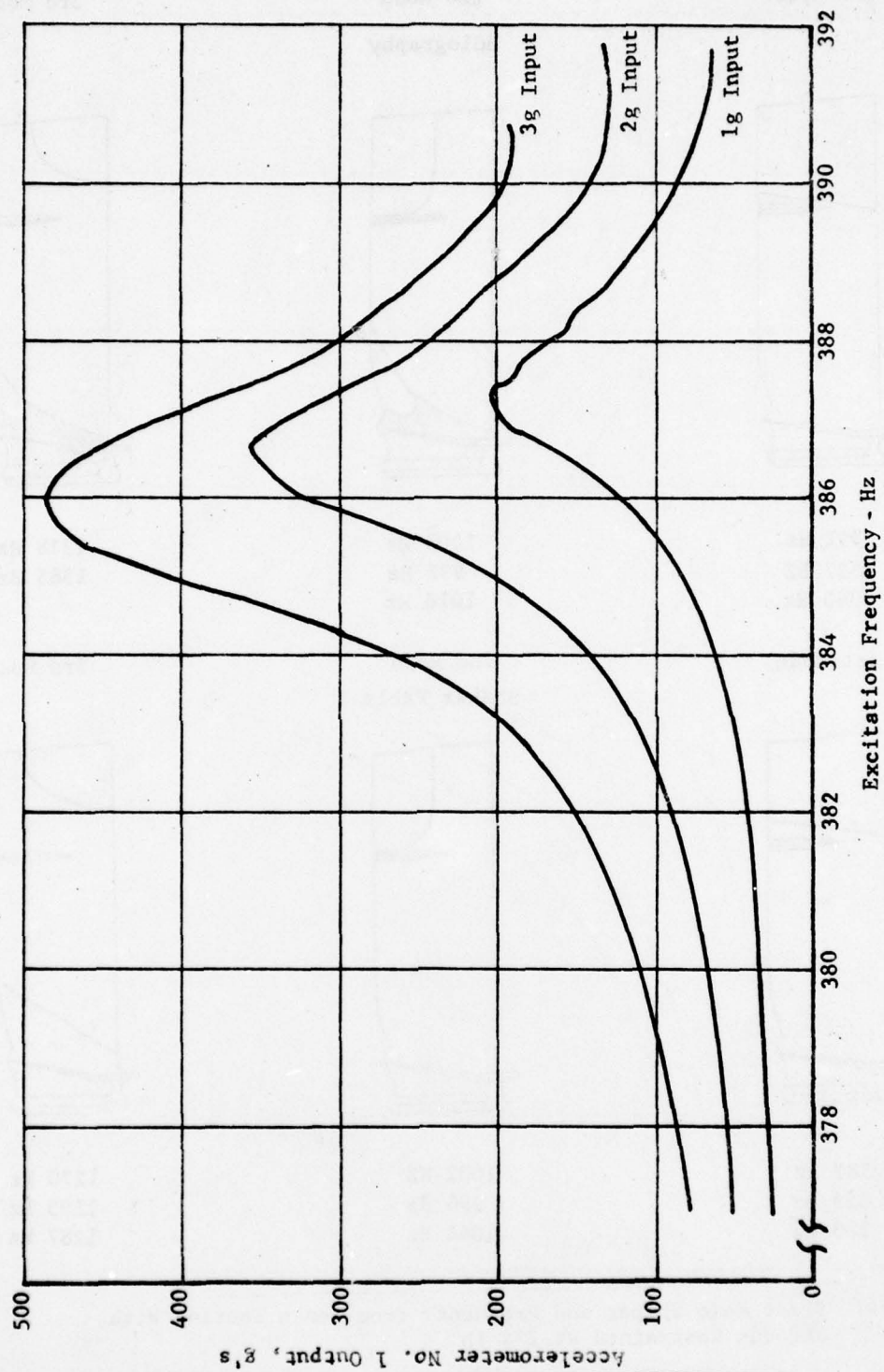


Figure 37. Blade Tip Response versus Frequency Shroud Load at 200 lb

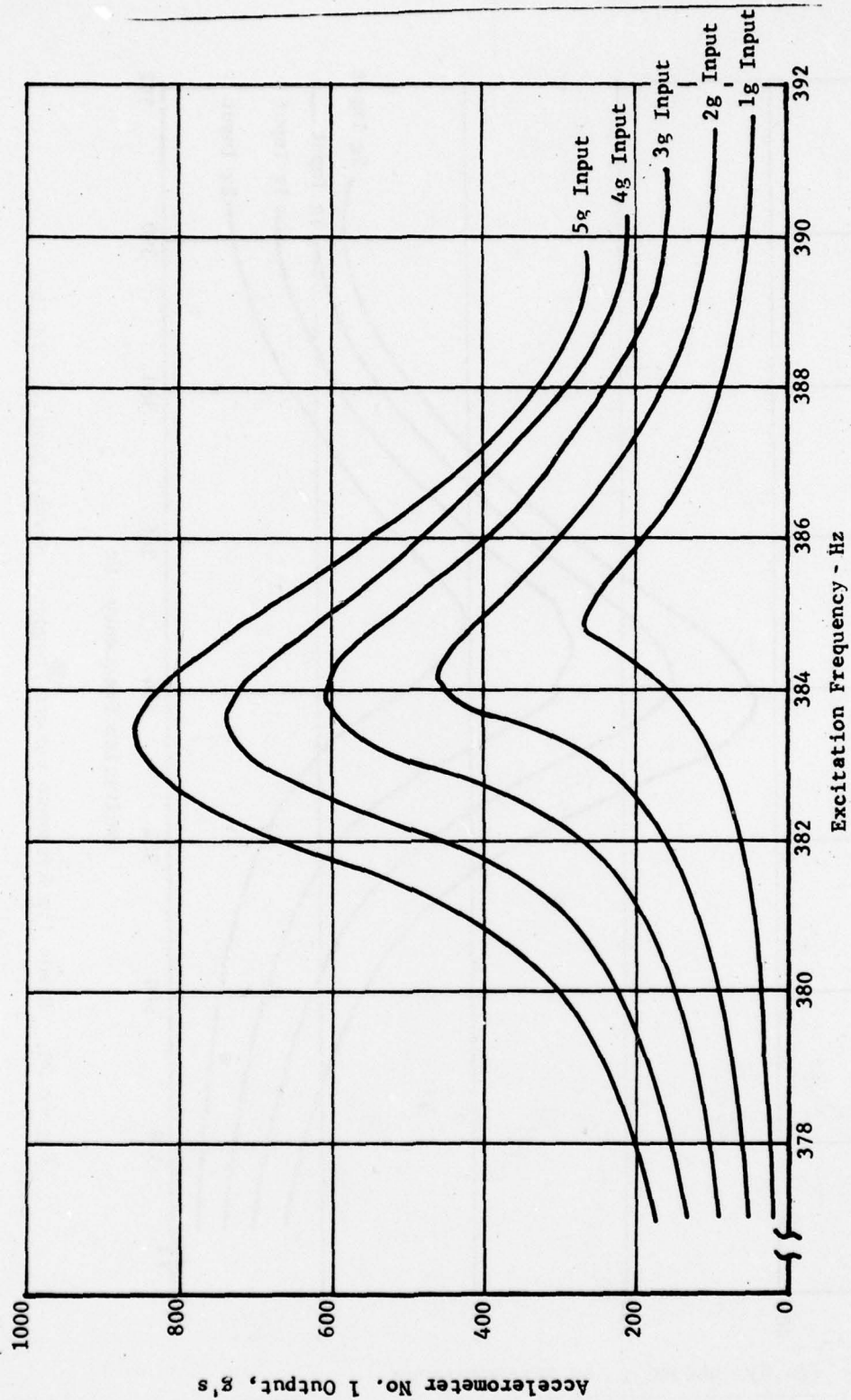


Figure 38. Blade Tip Response versus Frequency Shroud Load at 234 lb

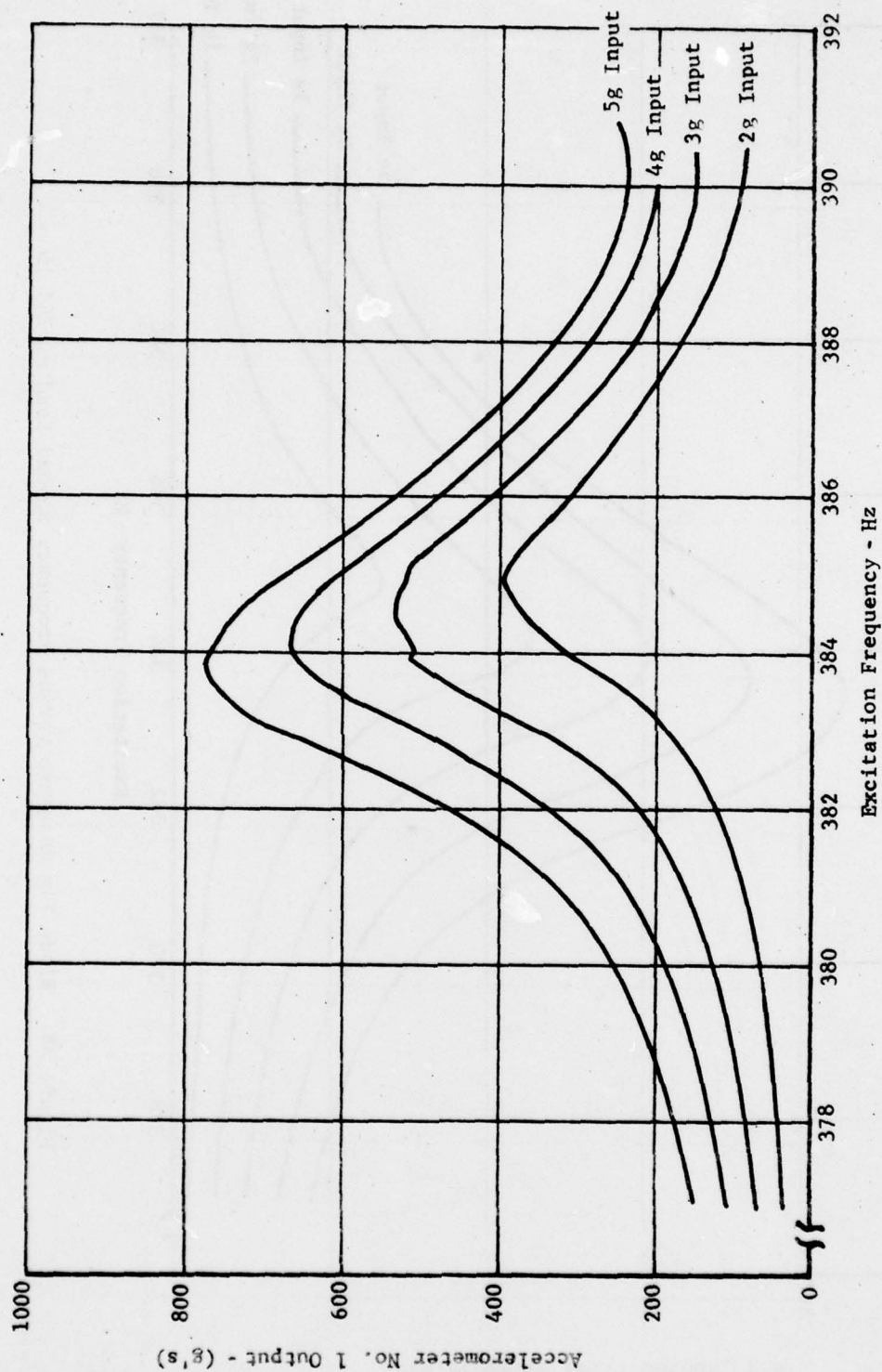


Figure 39. Blade Tip Response versus Frequency Shroud Load at 280 lb

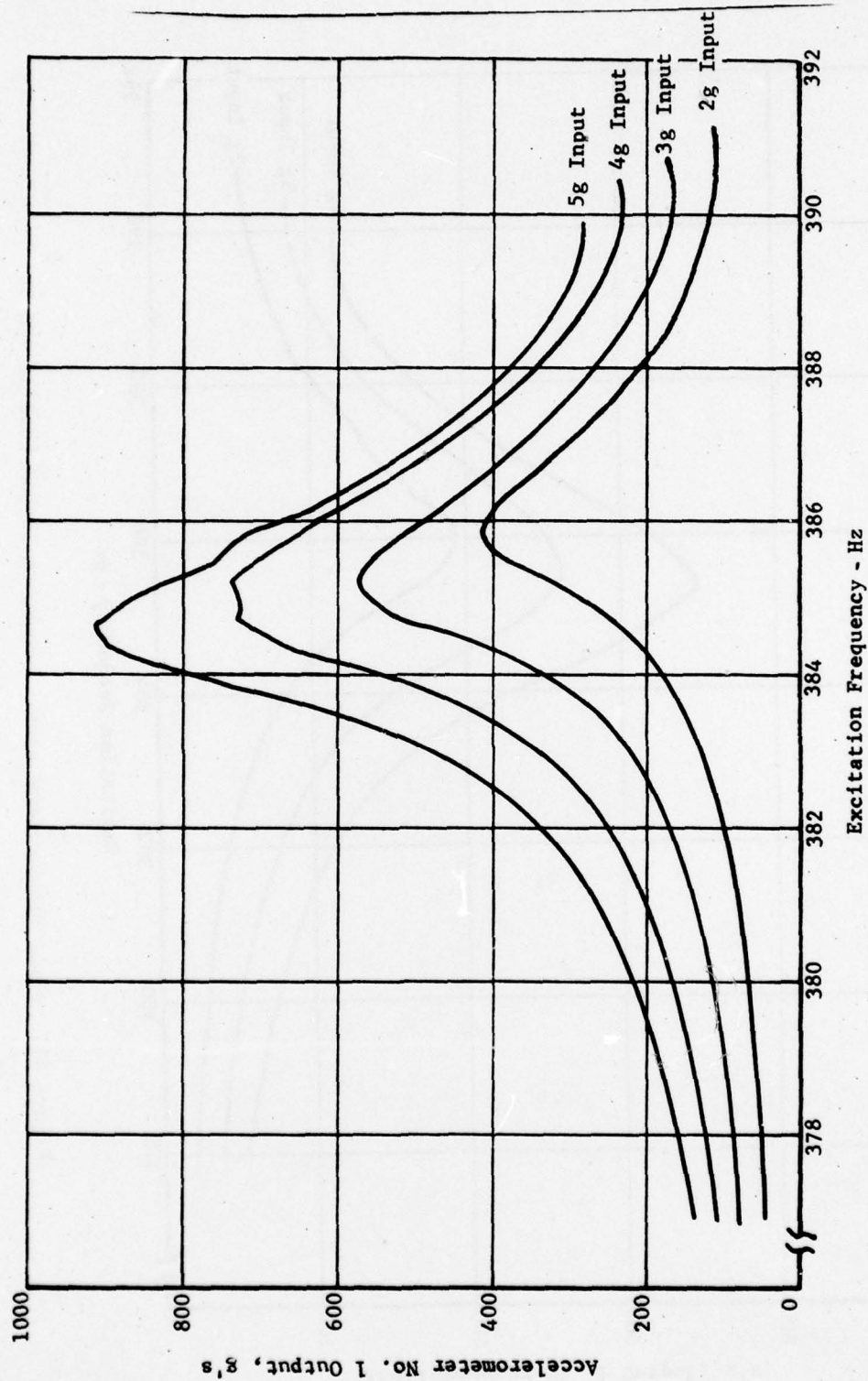


Figure 40. Blade Tip Response versus Frequency Shroud Load at 330 lb

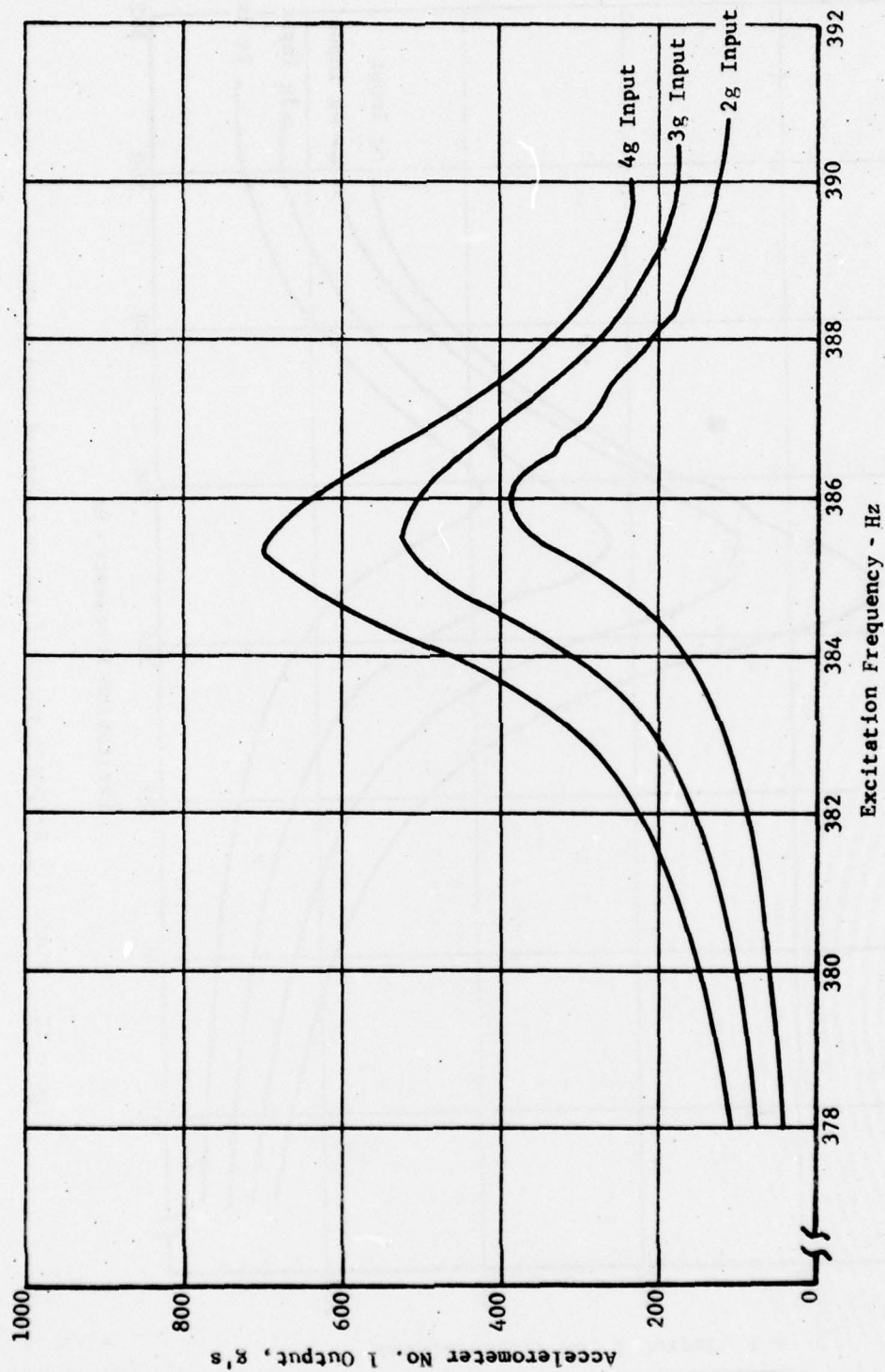


Figure 41. Blade Tip Response versus Frequency Shroud Load at 400 lb

41

DA
FILM

8 —